Casimir Togbé, Luc-Sy Tran, Dong Liu, Daniel Felsmann, Patrick Oßwald, Pierre-Alexandre Glaude, Baptiste Sirjean, René Fournet, Frédérique Battin-Leclerc and Katharina Kohse-Höinghaus, *Combustion chemistry and flame structure of furan group biofuels using molecular-beam mass spectrometry and gas chromatography – Part III: 2,5-Dimethylfuran*, Combustion and Flame, **161** (2014) 780-797.

The original publication is available at www.elsevier.com

http://dx.doi.org/10.1016/j.combustflame.2013.05.026

Combustion chemistry and flame structure of furan group biofuels using molecular-beam mass spectrometry and gas chromatography – Part III: 2,5-Dimethylfuran

Casimir Togbé[1], Luc-Sy Tran[2], Dong Liu[1], Daniel Felsmann[1], Patrick Oßwald[1#], Pierre-Alexandre Glaude[2], Baptiste Sirjean[2], René Fournet[2], Frédérique Battin-Leclerc[2*], Katharina Kohse-Höinghaus[1*]

[1] Department of Chemistry, Bielefeld University, Universitätsstraße 25, D-33615 Bielefeld, Germany

[2] Laboratoire Réactions et Génie des Procédés (LRGP), CNRS, Université de Lorraine, ENSIC, 1 rue Grandville, BP 20451, 54001 Nancy Cedex, France

[#] now at German Aerospace Center (DLR), Institute of Combustion Technology, Pfaffenwaldring 38-40, D-70569 Stuttgart, Germany

Supplemental Material is available.

[*] Corresponding authors. Katharina Kohse-Höinghaus: Email: kkh@uni-bielefeld.de, Phone: +49 521 106 2052, Fax: +49 521 106 6027 and Frédérique Battin-Leclerc: Email: Frederique.battin-leclerc@univ-lorraine.fr, Phone: +33 383175125, Fax: +33 383378120

Abstract

This work is the third part of a study focusing on the combustion chemistry and flame structure of furan and selected alkylated derivatives, i.e. furan in Part I, 2-methylfuran (MF) in Part II, and 2,5-dimethylfuran (DMF) in the present work. Two premixed low-pressure (20 and 40 mbar) flat argon-diluted (50%) flames of DMF were studied with electron-ionization molecular-beam mass spectrometry (EI-MBMS) and gas chromatography (GC) under two equivalence ratios (ϕ=1.0 and 1.7). Mole fractions of reactants, products, and stable and radical intermediates were measured as a function of the distance to the burner. Kinetic modeling was performed using a reaction mechanism that was further developed in the present series, including Part I and Part II. A reasonable agreement between the present experimental results and the simulation is observed. The main reaction pathways of DMF consumption were derived from a reaction flow analysis. Also, a comparison of the key features for the three flames is presented, as well as a comparison between these flames of furanic compounds and those of other fuels. An a priori surprising ability of DMF to form soot precursors (e.g. 1,3-cyclopentadiene or benzene) compared to less substituted furans and to other fuels has been experimentally observed and is well explained in the model.

Keywords: 2,5-dimethylfuran, low-pressure flame, model, reaction mechanism, reaction flow analysis, molecular-beam mass spectrometry, gas chromatography.

1. Introduction

Biofuel, as a fuel category, is a renewable resource and, although different classes of fuels belong to this category, biofuel is generally thought to hold a promising future [1,2]. Ethanol, the only renewable liquid fuel currently produced in large quantities, has been the subject of numerous publications [3-9], but it suffers from several limitations, including comparatively low energy density, high volatility, and high energy consumption for its production. The search for alternatives to ethanol has become a primary research target. Recent developments have focused their attention on 2,5-dimethylfuran (DMF) as a possible alternative transportation fuel which can be produced from biological sources [10-13]. Also it can be produced by biotechnological methods [14]. DMF offers several advantages over the current biofuel ethanol, including its 40% higher energy density which is close to that of gasoline [15].

Combustion of DMF has been investigated in engines [15-17] and its pyrolysis and oxidation have also been studied [18,19]. Wu et al. [20] have analyzed DMF/oxygen/argon flames at low pressure (40 mbar) and an equivalence ratio of 2.0 with tunable vacuum ultraviolet (VUV) synchrotron radiation photoionization and molecular-beam mass spectrometry. Their work reports intermediate species identification in the combustion of DMF, and they showed that furan and 2-methylfuran are stable intermediate species in the low-pressure DMF flames. Based on their identification of species, they also proposed possible reaction pathways for the decomposition of furans. Quantitative species profiles were not provided, however. Tian et al. [21] have investigated the laminar flame speed of DMF in the range of equivalence ratios ϕ from 0.6 to 2.0 and initial temperatures from 323 to 373 K. Their study showed that, for ϕ=0.9-1.1, DMF laminar flame speeds are different from those of gasoline by ~10%. Also, Wu and co-workers [22] measured laminar burning velocities and Markstein lengths of DMF-air premixed mixtures at different temperatures.

Quantum chemical calculations for the DMF system were recently also reported [23,24]. Simmie and Metcalfe [23] employed *ab initio* methods to calculate energies and kinetic rate coefficents for several unimolecular decomposition pathways and free radical reactions involving DMF. They concluded that hydrogen atom migrations to form singlet carbenes are important in the decomposition of these species. Friese et al. [24] studied the thermal decomposition of DMF to form hydrogen atoms and the corresponding radical as well as the DMF + H reaction behind reflected shock waves; these experiments were performed at 1280-1520 K and 980-1250 K, respectively, at pressures of 1.6 and 4.7 bar. The authors concluded that the principal pathway was an addition-elimination mechanism to yield MF and the methyl radical. Most recently, the reaction of DMF with H-atoms has also been studied by Sirjean and Fournet [25,26] using a potential energy surface calculated at the CBS-QB3 level of theory and master equation/RRKM modeling. The major product channels of this reaction observed in that work are the ipso-substitution DMF + H to form MF and the methyl radical as well as the formation of 1,3-butadiene and the acetyl radical (CH_3CO). Sirjean and Fournet [27] performed similar investigations for the 5-methyl-2-furanylmethyl radical via theoretical calculations and master equation/RRKM modeling. Note that the 5-methyl-2-furanylmethyl radical is the most important primary radical formed during the combustion and thermal decomposition of DMF. In their study, pressure-dependent rate coefficients were proposed for pressures from 0.01 bar to 10 bar and temperatures from 1000 K to 2000 K. Using the results of these theoretical investigations, Sirjean et al. [28] have proposed a detailed kinetic model for the oxidation of DMF validated under shock tube conditions (T=1300-1813 K) and using pyrolysis data of Lifshitz et al. [19].

While some detailed information on the combustion of DMF is thus available, a quantitative comparison of flame species profiles with a dedicated chemical kinetic mechanism is, to the best of our knowledge, still lacking. In view of the interest in furan and its derivatives as alter-

native transportation fuels, the present series of experiments of low-pressure furan flames in Part I [29] and 2-methylfuran flames in Part II [30] is now followed by measurements of DMF combustion for two flame stoichiometries under identical conditions as for the other two fuels investigated before. Also, a single model has been developed and tested for all three fuels and six flame conditions. With this consistent approach, it is believed that the knowledge of the combustion of furanic fuels has been considerably advanced, and that further model development including this data may also serve as a basis for transfer of this knowledge to combustion conditions more representative of practical application.

2. Experimental results

The experimental facilities in Bielefeld and Nancy used in this study have been described in detail in [31-33] and in Part I [29]; such details will, therefore, not be reported here again.

Premixed low-pressure (20 mbar and 40 mbar) flat argon-diluted (50%) flames of DMF were investigated for two equivalence ratios (ϕ=1.0 and 1.7). Flame conditions are presented in Table 1. Hydrocarbon and oxygenate species were measured with two methods: Online gas chromatography (GC) was used in Nancy to provide isomer-specific information for stable intermediates, whereas electron-ionization molecular-beam mass spectrometry (EI-MBMS) was performed in Bielefeld to provide stable, radical, and intermediate species. Temperature was derived from the pressure in the first pumping stage by a procedure described in Part I [29] and calibrated at a height of 25 mm above the burner from CO/CO_2 absorption measurements with a quantum cascade laser using tomographic reconstruction [29]. The temperature profile obtained this way traces the fate of a gas sample withdrawn by the probe and is therefore called "perturbed" temperature profile here. When this perturbed temperature profile is used as input for the simulations, no shifts between experimental and modeling profiles have to be applied.

While the study of Wu et al. [20] has been considered as the first analysis of DMF combustion under laminar premixed low-pressure flame conditions, no mole fraction profiles were reported. The present work could then be considered as the first measurement with mole fraction profiles provided.

Figures 1-6 show the mole fraction profiles (EI-MBMS) of reactants, selected intermediates and products for the fuel-rich flame (ϕ=1.7). Analogous results for the stoichiometric flame can be found in the Supplemental Material (Figs. S1-S5). Exemplary results from GC identification are presented in Figs. 7 and 8. For all important intermediate species, a summary of experimental results is given in Tables 2 and 3. This new set of experimental data from premixed DMF low-pressure flames was used as a basis for detailed chemical kinetic modeling.

For major species presented in Fig. 1, including Ar, O_2, CO, CO_2, H_2O, and fuel, the global combustion behavior is very similar to that found for furan [29] and MF [30]. The measured exhaust gas composition near 43 mm reaches the thermodynamic equilibrium values (open symbols) calculated with Gaseq [34] for the respective flame temperature. The mole fractions of CO and H_2 measured in the fuel-rich flame are larger than those obtained in the stoichiometric flame and remain constant along the post flame region.

For intermediate species (Figs. 2-6 and S1-S5), acetylene (C_2H_2) is the most abundant one with maximum mole fractions of up to 3.1×10^{-2} and 1.4×10^{-2} in the fuel-rich (Fig. 2) and stoichiometric flame (Fig. S1), respectively. An excellent agreement between GC and MBMS measurements can be observed for this species (Table 3). Methane (CH_4), ethene (or ethylene, C_2H_4), and ethane (C_2H_6) are measured with maximum mole fractions of 4.4×10^{-3}, 7.1×10^{-3}, and 3.0×10^{-3} in the fuel-rich flame, respectively (Fig. 2).

Among C_3 hydrocarbon intermediates (Figs. 3 and S2), the mole fraction of C_3H_4 is the largest with maximum values of 3.8×10^{-3} and 2.5×10^{-3} in the fuel-rich and stoichiometric flame, respectively. This trend was also found in the furan [29] and the MF flames [30]. In the

stoichiometric flame, the most abundant C_4 species is C_4H_6 (maximum mole fraction of 2.4×10^{-3}, Fig. S2), and it is C_4H_2 in the fuel-rich flame (maximum mole fraction of 4.2×10^{-3}, Fig. 3). While the mole fraction of most C_4 hydrocarbon intermediates are enhanced by increasing equivalence ratio, that of C_4H_8 decreases. C_4H_8 reaches its maximum at 3 mm with mole fractions of 6.7×10^{-4} (ϕ=1.0) and 4.1×10^{-4} (ϕ=1.7). C_5H_6 and C_6H_6 are the most abundant species of the C_5 and C_6 hydrocarbon intermediates with maximum mole fractions of 2.5×10^{-3} and 1.0×10^{-3} in the fuel-rich flame (Fig. 4). For oxygenated intermediates (Figs. 5, 6, S4, and S5), CH_2O (formaldehyde) and C_5H_6O (methylfuran) are detected with a large mole fraction of $\sim3.0\times10^{-3}$ and $\sim2.5\times10^{-3}$. C_6H_6O (phenol) is also an abundant intermediate with a mole fraction of up to $\sim1.0\times10^{-3}$.

The composition of isomers is an interesting feature in the comparison of the present DMF flames (Table 3 and Figs. 7 and 8) and those obtained in the furan (Table 4 in Ref. [29]) and MF (Table 3 in Ref. [30]) flames. For example, similarities exist with propyne as the dominant isomer of C_3H_4 (propyne and allene); C_4H_6, C_4H_8, and C_5H_{10} are predominantly 1,2-butadiene, 1-butene, and 2-pentene in all these flames and C_5H_6 and C_2H_4O are mostly 1,3-cyclopentadiene and acetaldehyde, again for all three fuels. However, the composition of C_4H_6O measured in the DMF flames (where 2-butenone is the most abundant isomer) is similar to that found in the MF flames [30], but different to that obtained in the furan flames [29], where 2-butenal is the most abundant one. Also, the composition of C_4H_8O obtained in the DMF flames is different to that found in both furan and MF flames. In the furan [29] and MF [30] flames, isobutanal and 2-butanone were measured as the two isomers of C_4H_8O, with the largest mole fraction for isobutanal, while isobutanal was not detected in the DMF flames.

In comparison with the species identifications in the work of Wu et al. [20], some species were similarly identified by both studies, such as propyne (pC_3H_4), allene (C_3H_4), 1-butene-3-yne (vinylacetylene, C_4H_4), 1,3-cyclopentadiene (C_5H_6), benzene (C_6H_6), acetaldehyde

(C_2H_4O), furan (C_4H_4O), and 2-methylfuran (C_5H_6O). However, some identifications are different, especially for some oxygenated species. For example, C_2H_6O was identified as dimethylether in the present work, whereas it was not detected in the study by Wu el al. [20]. Also, the composition of C_4H_6O includes 2-butenone, 2-butenal, and 2,3-dihydrofuran in this study, whereas C_4H_6O was identified by Wu et al. [20] as 2,5-dihydrofuran and ethenyl oxirane. Furthermore, C_4H_8O is seen to be 2-butanone and isobutanal in this work, whereas it was detected as tetrahydrofuran by Wu et al. [20]. As another example, C_5H_8O was identified here as 3-pentene-2-one, but in Ref. [20] it was detected as 2,5-dihydro-2-methylfuran. This highlights the advantage of using independent methods for species identification, as was done here. Also, C_4H_8 and C_5H_8 which were not observed in the study by Wu et al. [20], were detected in the present work. Note that an overall good agreement between GC and EI-MBMS measurement in the present work was observed for all these species (except for C_4H_6O with a disagreement by about a factor of 4 which is higher than the error limit of the calibration method for this species). However, the complex composition of the signal (for isomers) and the respective calibration in this case may increase the acceptable error tolerance here. In the GC measurement, three other cyclic compounds including styrene (C_8H_8), ethyl benzene (C_8H_{10}), and 2-ethyl-5-methyl furan ($C_7H_{10}O$) were also detected. Other species, for which the nominal mass is higher than that of DMF (*m/z*=96), were detected but not quantified in the EI-MBMS measurement because the signal intensities were too small.

3. Kinetic modeling

Kinetic modeling of the premixed flat laminar DMF flames was performed using the CHEMKIN package with the PREMIX code [35]. The kinetic reaction mechanism used here with 305 species and 1472 reactions is an extended version of that proposed for the oxidation of DMF [28]. Because preliminary tests demonstrated that the set of furan and MF sub-mechanisms in

Ref. [28] was not able to accurately reproduce the new set of furan and methylfuran experiments, the original mechanism scheme was revised to provide better agreement with furan [29] and methylfuran data [30]. However for DMF, the sub-mechanism of Ref. [28] was adopted without any change. The model is built in a hierarchical and systematic way. It includes: (i) unimolecular initiations by breaking of a C-C or C-H bond in the lateral methyl groups, by H-atom or CH_3 transfer, and by ring opening at the C-O bond; (ii) bimolecular initiation with O_2 or bimolecular initiation between two molecules of DMF; (iii) propagation reactions by H-abstractions from the methyl groups and the furan ring and by H-addition and OH-addition on double bonds; and (iv) the subsequent decomposition of the formed products. In the present work, low-pressure coefficients were used in the case of pressure-dependent rate coefficients. It is important to note that the high-pressure rate coefficients of Sirjean et al. [28] need to be used for simulation of data under high-pressure conditions.

The mechanism, thermodynamic and transport data are available in CHEMKIN format in the Supplemental Material of Part I [29].

4. Comparison between experimental and simulated results

4.1. Major species

Major species mole fraction profiles are presented in Fig. 1 together with the respective perturbed temperature profiles (broken lines) which were used as input parameters for the model. It is worth noticing that no shifts were applied between profiles from experiment and simulations. In general, the profiles of major species shown in Fig. 1, including DMF, O_2, H_2, CO, CO_2, and H_2O, are well predicted by the model. This agreement is satisfactory for the profile shape as well as for the mole fraction values. Note that small discrepancies between prediction and experiment are observed for the mole fraction values for the H_2O profile (~12%) in the

stoichiometric flame and for the CO_2 profile (~15%) in the fuel-rich flame beyond 6 mm; but this is within the experimental error range.

4.2. Intermediate species

The experimental profiles of the intermediate species and the respective simulation will be discussed for both equivalence ratios, ϕ=1.0 and 1.7. The figures for ϕ=1.7 are presented here, the analogous figures for the stoichiometric flames can be found in the Supplemental Material.

Figures 2-4 and S1-S3 display a comparison between experimental and simulated data for hydrocarbon intermediates in the two DMF flames. Overall, the agreement between prediction and experiment is quite good. However, the simulation for some species is not as satisfactory and needs further discussion.

The model tends to overpredict the maximum mole fractions of the radicals CH_3 and C_2H_5 by a factor of 3-4 and underpredicts that of C_3H_5 by a factor of ~1.5 (Figs. 2-3 and S1-S2). The mole fraction profile of C_3H_5 is the sum of the allyl (C_3H_5-Y), 1-methyl vinyl (C_3H_5-T), and 2-methyl vinyl (C_3H_5-s) radicals. In the EI-MBMS experiment, the calibration factors for the three radicals CH_3, C_2H_5, and C_3H_5 are determined by RICS from CH_4, C_2H_6, and C_3H_6, respectively (Table 2). The typical error of this calibration method can be up to a factor of 2-4 for radicals. Therefore, the agreement can be considered as still within the expected experimental uncertainties for these radicals.

The isomers allene (aC_3H_4) and propyne (pC_3H_4) are not distinguishable in the EI-MBMS experiment but can be separated in the GC analysis. Therefore, EI-MBMS provides the sum of both isomers. A discrepancy of about a factor of 2.5 between prediction and EI-MBMS experiment is observed for the mole fraction value of C_3H_4 (Figs. 3 and S2), while simulation and the GC measurement are in better agreement. The ratio between propyne and allene is ~1.87 for the simulation and ~1.97 in the GC measurement as shown in Table 3.

Diacetylene (C_4H_2) is well predicted in the stoichiometric flame (Fig. S2), but underpredicted by about a factor of 2 in the fuel-rich flame (Fig. 3). Trends in the furan [29] and MF [30] flames are slightly different. The formation of vinylacetylene (C_4H_4) was predicted reasonably well by the model in the furan and MF flames [29,30], whereas it is underpredicted by about a factor of 4 in the DMF flames (Figs. 3 and S2). In the fuel-rich flame, a good agreement between EI-MBMS and GC measurements is observed for the maximum mole fraction of C_4H_4 (see Table 3). The lower amount of C_4H_4 in the simulation could result from the uncertainty in the fall-off coefficients for the unimolecular initiation reaction (R30) in the following reaction pathway:

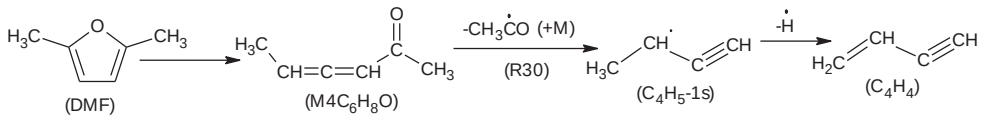

Sirjean et al. [28] showed that this reaction pathway is the main decomposition channel leading to the formation of C_4H_4 under the DMF pyrolysis conditions of Lifshitz et al. [19] at pressures >1 bar. Furthermore, the mole fraction of C_4H_4 was well predicted in [28] for the DMF pyrolysis results of Lifshitz et al. [19]. As discussed by Sirjean and Fournet [26], reaction (R30) depends strongly on pressure, especially below 1 bar, but its Troe coefficients were adapted from the calculations of Klippenstein et al. [36] for the reaction toluene→phenyl+CH_3. For pressures below 1 bar, the uncertainty in these parameters for reaction (R30) was estimated to be at least a factor of 3 [26], which could contribute to the underprediction of the C_4H_4 formation in the present low-pressure flames. Further experimental and theoretical studies will be necessary to establish more accurate pressure-dependent branching ratios. Moreover, the discrepancy between the experimental and simulated mole fraction of C_4H_4 could also result from the reaction database. Indeed, several reactions involving the formation of C_4H_4 from unsaturated species (such as from aC_3H_4, pC_3H_4 via the formation of C_3H_3, or from 1,3-C_4H_6 via the formation of C_4H_5) are considered in the reaction base but some of them are still unsatisfactorily described.

The C_4H_8 mole fraction is predicted in excellent agreement for the stoichiometric flame (Fig. S2) and reasonably well in the fuel-rich flame (Fig. 3). GC analysis reveals the composition to be mainly 2-butene with a lower mole fraction of 1-butene (Fig. 7), with MBMS and GC results in quite good agreement for the global mole fraction; the simulation predicts a slightly different partition of these two isomers, with almost similar contributions of the two butane isomers. The second peak seen in the MBMS measurements is probably an experimental artifact.

Mole fractions of C_5H_8 are in good agreement for the fuel-rich flame (Fig. 4) and underpredicted by about a factor of 2 in the stoichiometric flame (Fig. S3). The isomer composition from the GC experiment is reported in Fig. 8 (and Table 3) and includes isoprene, 2-pentyne, and 1,3-pentadiene. The latter is the dominant isomer in the measurements, while the model predicts the highest contribution to be 2-pentyne. This composition is somewhat different from that in the fuel-rich MF flame [30] where isoprene plays a similarly important role as 1,3-pentadiene in the measurements and in the simulation.

The mole fraction of C_5H_{10} which is the sum of 2-pentene, 3-methyl-1-butene, and 1-pentene is quite well predicted by the model in the stoichiometric DMF flame (Fig. S3), but overpredicted by a factor of 3.5 in the fuel-rich flame (Fig. 4). In EI-MBMS, C_5H_{10} is calibrated as 2-pentene, since this species is the most abundant one of the three isomers of C_5H_{10} detected by GC (Table 3). As shown in Table 3, in the fuel-rich flame the mole fraction of C_5H_{10} quantified by EI-MBMS is lower than that quantified by GC (by about a factor of 5) which is close to the simulated peak of C_5H_{10}. The uncertainty in the EI-MBMS data evaluation for C_5H_{10} in the fuel-rich DMF flame could explain this disagreement of C_5H_{10} profile.

Figures 5, 6, S4, and S5 display a comparison between experimental and simulated data for some selected oxygenated intermediates in the two DMF flames (ϕ=1.0 and 1.7). These figures

show that the mole fraction profiles of CH_2O, C_2H_2O, C_2H_6O, C_3H_6O, C_4H_4O, C_5H_6O, and C_6H_6O are reproduced reasonably well by the model within the experimental error limits.

As shown in Table 3, good agreement between EI-MBMS and GC measurements is observed for the maximum mole fraction of C_2H_4O (mostly acetaldehyde, CH_3CHO), but it is overpredicted by the model, especially in the stoichiometric flame. According to the rate of production (ROP) analysis, CH_3CHO is mainly formed by OH-addition to DMF ($DMF+OH \rightarrow CH_3CO+CH_3CHO+C_2H_2$). In the absence of literature reports for this quite complex elementary reaction, as discussed in Ref. [28], this process has been taken into account assuming that it leads ultimately to the formation of the CH_3CO radical, acetaldehyde, and acetylene. The rate coefficient of this reaction has been considered to be similar to that of furan+OH, measured by Atkinson and Arey [37] at the high-pressure limit. The uncertainty in the rate coefficient of this reaction could result in the overprediction of the CH_3CHO formation at low pressure.

The formation of C_3H_4O and C_4H_6O is also underpredicted by the model. Note that, in the EI-MBMS experiment data, C_4H_6O is calibrated as 2-butenone, since this species is the most abundant one of the three isomers of C_4H_6O, namely 2-butenone, 2-butenal, and 2,3-dihydrofuran detected by GC (Table 3). As 2-butenone and 2-butenal were not included in the model, this may explain the underprediction of the C_4H_6O profile.

To investigate the effect of the addition/revision of reactions in the furan and MF submechanisms on the overall simulation results of DMF, the previous DMF model of Sirjean et al. [28] (switched to low-pressure rate coefficients) was also used to simulate the present data and then compared to the present model. The results show that, overall, there is not much difference between both simulations (see the species in Fig. S6 in the Supplemental Material as examples). Differences are found only for a few species, always by less than a factor of two. Indeed, by the effect of added/revised reaction pathways, with the present model the simulated

mole fractions of MF (C_5H_6O) and furan (C_4H_4O) decrease by factors of ~1.2-1.7, that of acrolein (C_3H_4O) decreases slightly, while those of C_2H_4, C_3H_5, C_3H_6, and C_4H_4 increase by factors of 1.3-1.5, and those of C_4H_6, CH_2O, and C_3H_6O increase slightly. Note that the changes concerning most of these species tend to improve the simulated profiles. The profiles of other species remain almost unchanged.

The present model was successfully validated against experimental low-pressure flame data. However, it can be noted that uncertainties in rate coefficients may impact the overall simulation results; this holds especially for those of the most sensitive reactions. A full quantification of uncertainties in the simulations is beyond the scope of this work. Sensitivity analyses for the conversion of the fuels (DMF, MF, and furan) and for the formation of the most important pollutants (Table 5) should point out which reaction rate uncertainties should be further reduced to improve the overall speciation modeling. In the model, rate coefficients were determined using three methods: theoretical calculations, estimations, and review of the literature. The uncertainties in rate coefficients are less than a factor of three for the first category (theoretical calculation), but larger for the second category (estimation). For the third category (review of the literature), uncertainties depend on the specific method used to determine rate coefficients ineach work, and the references could be consulted directly for each reaction. Note that the rate coefficients of most reactions of DMF which are presented in the reaction rate analyses have been theoretically calculated [25], while those of the reactions of MF have been estimated by analogies with DMF and furan reactions [28,30]. Uncertainties in rate coefficients of some other specific reactions and their effects on the formation of intermediates, for instance the absence of information for O- and OOH-additions to furanic fuels, and of OH-addition to MF, have been analyzed in the discussion sections of the three papers.

5. Reaction pathways of DMF combustion

The simulated main flows of consumption of DMF under flame conditions, based on the ROP analysis of the present model, are shown in Fig. 9 for the fuel-rich flame at *h*=3.1 mm from the burner, corresponding to a temperature of 1101 K and a simulated conversion of DMF of 73%. Please note that the structures for all species discussed in this section can be found in Table 4.

For these conditions, the most important channel of consumption of DMF (~42%) is H-abstraction by H, OH, O, and CH_3 from the methyl group to yield the resonance-stabilized 5-methyl-2-furanylmethyl radical ($R1C_6H_7O$). The dominant pathway of DMF consumption starting from this radical yields the stable products 1,3-cyclopentadiene and phenol which are well predicted; see the more detailed analysis below. Figure 10 shows that the C-H bond energy in the methyl group of the DMF molecule is much lower than that of the C-H bond in the furan ring and that of C2-C6 (or C5-C7) bonds. A second important channel of consumption of DMF is the ipso-addition yielding MF (C_5H_6O) and CH_3 (~30%). About 21% of DMF is consumed by H-addition at the C2 position of DMF; this is followed by the rearrangements of the initial stabilized adduct which then ultimately yields 1,3-butadiene (1,3-C_4H_6) and the acetyl radical (CH_3CO); the latter decomposes mainly into CO and CH_3 (~95%) or reacts with CH_3 to form ketene (C_2H_2O) and CH_4 (~4%). The C_4H_6 profile is well reproduced by the model (Figs. 3 and S2). A minor channel of consumption of DMF is OH-addition to the C2 position of DMF to form acetaldehyde (CH_3CHO), acetylene (C_2H_2), and the CH_3CO radical. The contribution of other channels to the consumption of DMF under these conditions is very small (<1%).

MF (C_5H_6O) reacts via several pathways, as discussed in the respective section of Part II [30] of this series. In short, the ipso-addition yields furan (C_4H_4O) and the CH_3 radical; H-addition to MF yields the but-1-en-1-yl radical (C_4H_7-V, CH_3─CH_2─CH=CH) and CO or 1,3-butadiene (1,3-C_4H_6) and CHO; H-abstractions from the methyl group of MF result in the resonance-stabilized 2-furylmethyl radical (furylCH_2); H-abstraction from the furan ring produces the 2-methylfuran-5-yl radical (M5F-2yl). MF is an important primary product in the

DMF reaction. Thus, the revision in the MF sub-mechanism, described in Part II [30], plays an important role for the DMF simulation. The MF profile is quite well predicted by the model (Figs. 6 and S5).

The ring opening of the stabilized R1C_6H_7O radical involves the formation of the R2C_6H_7O radical, followed by an internal H-atom transfer to form the R3C_6H_7O radical. The R3C_6H_7O radical then reacts mainly by C_6 ring enlargement to form the R4C_6H_7O radical. A minor channel of consumption of R3C_6H_7O is a C_3 ring closure leading to the R5C_6H_7O radical. This R5C_6H_7O radical opens by β-scission of the C-C bond of the ring followed by a CO- elimination to produce the stabilized C_5H_7Y radical which forms the cyclopent-2-en-1-yl radical (C_5H_7#Y) by ring closure or 1,3-pentadiene (1,3-C_5H_8) by recombination with an H-atom.

For the R4C_6H_7O radical, β-scission of the C-H bond or reaction with an H-atom are important channels and lead to the formation of cyclohexa-2,4-dien-1-one (M2C_6H_6O) which then converts into cyclohexa-2,5-dien-1-one (M3C_6H_6O) via the formation of a biradical (B1C_6H_6O) or into phenol (C_6H_6O), either directly or via the formation of the phenoxy radical (C_6H_5O#). Two other pathways of consumption of the R4C_6H_7O radical are a ring opening leading to R9C_6H_7O which, in turn, reacts by CO-elimination to form the C_5H_7#Y radical and an internal H-atom shift leading to the production of the R6C_6H_7O radical.

The ring opening of the R6C_6H_7O radical followed by a CO-elimination leads to the formation of the penta-1,4-dien-1-yl radical (C_5H_7-1s). This C_5H_7-1s radical can decompose into C_2H_2 and the allyl radical (C_3H_5-Y) by β-scission of the C-C bond, but most of it is consumed by ring closure to form the cyclopent-3-en-1-yl radical (C_5H_7#) which then reacts by isomerization to form the C_5H_7#Y radical or decomposes into 1,3-cyclopentadiene (1,3-C_5H_6) and an H-atom. The R6C_6H_7O radical leads also to M2C_6H_6O or M3C_6H_6O by β-scission of the C-H bond.

M3C_6H_6O, formed from R_6H_7O or M2C_6H_6O, is consumed mainly by H-abstractions to form the phenoxy radical (C_6H_5O#). This latter converts to phenol by reacting with an H-atom, to 1,3-C_5H_6, or to the cyclopentadienyl radical (C_5H_5#) via the formation of a bicyclic radical followed by a CO-elimination.

This analysis explains why 1,3-cyclopentadiene and phenol were detected with substantially higher mole fractions (by a factor of 10-30 for 1,3-cyclopentadiene and of 20-100 for phenol; see Table S1 in the Supplemental Material) compared to those in the furan and MF flames. The formation of these two species is well predicted by the model (Figs. 4, 6, S3, and S5). Both species may serve as benzene precursors and could thus explain the extraordinarily high concentration of benzene detected in this flame.

In addition, it is worthwhile discussing the reaction pathways for the formation of some selected species that are not shown in Fig. 9.

An important part of ethene (or ethylene, C_2H_4), which is well predicted by the model (Figs. 2 and S1), is formed from the following reaction pathway starting from MF which is a primary product of the decomposition of DMF:

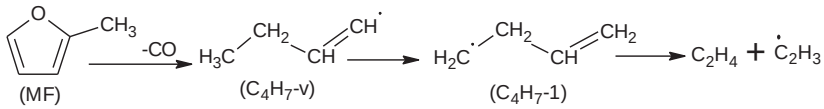

Ethane (C_2H_6) is produced by a combination of two CH_3 radicals and consumed mainly by H-abstractions which yield the C_2H_5 radical. The combination of the C_2H_3 and CH_3 radicals and that of the allyl radical (C_3H_5-Y) with an H-atom are involved in the formation of propene (C_3H_6). Diacetylene (1,3-butadiyne, C_4H_2) is mainly produced by the reaction $C_2H_2+C_2H=C_4H_2+H$, and mainly consumed by the reaction with an OH radical to form CHO and the C_3H_2 radical ($C_4H_2+OH=CHO+C_3H_2$).

1-butene (1-C_4H_8), which is the most abundant of the two isomers of C_4H_8 detected by GC (see Table 3), is formed by the combination of the C_3H_5-Y and CH_3 radicals

(C_3H_5-Y+CH_3=1-C_4H_8), as well as of an H-atom and the C_4H_7-Y radical (CH_2=CH─CH-CH_3). Note that C_4H_7-Y is obtained mainly by H-addition on 1,3-C_4H_6 which is a primary product of the decomposition of DMF (Fig. 9). The C_4H_8 profile is well predicted by the model (Figs. 3 and S2). C_6H_2 is formed from the reaction of C_4H_2 and the C_2H radical. Dimethyl ether (C_2H_6O) results from a combination of the CH_3O and CH_3 radicals, and is mainly consumed by H-abstractions. Propanal and acetone (C_3H_6O) are mainly formed by the reactions CH_3+CH_2CHO and CH_3+CH_3CO, respectively. As seen in Fig. 9, the CH_3CO radical is a primary product of the DMF decomposition by H- and OH-addition to DMF. The model well predicts the C_3H_6O profiles (Figs. 5 and S4).

The reaction pathways were also analyzed in the stoichiometric DMF flame and the same reactions are involved in the consumption of DMF with small differences in their respective importance. Indeed, when the equivalence ratio decreases, the importance of reactions involving oxygenated reactants, i.e. O-atoms, OH radicals, is somewhat enhanced.

6. Comparison of mole fraction profiles of potential pollutants

6.1. Comparison of the DMF flame with MF and furan flames

This paper is the third and last part of an experimental and numerical investigation of the combustion chemistry of premixed laminar flames of furan [29], 2-methylfuran [30], and 2,5-dimethylfuran (present work). It is interesting to compare the combustion of these three fuels regarding the mole fractions of products formed in the flames of these fuels burnt under similar conditions.

In general, the major species profiles for the three fuels are relatively similar regarding fuel consumption and main products (H_2, CO, CO_2, and H_2O), with the different stand-off distances reflecting the differences in flame speed. The detailed reaction pathways, however, depend on

the different fuel structures. In a comparison between the three fuels, intermediate species profiles and maximum mole fractions show some fuel specificity. Differences in the observed intermediates and in the measured maximum amounts merit further discussion. A summary of experimental results is given in Table S1 (Supplemental Material) that reports the maximum mole fractions of all measured intermediate species in the six flames of the three fuels.

Before discussing the differences in the formation of some specific intermediates between the three fuels, the influence of the structure of these fuels, presented in Fig. 10, should be taken into account. Bond dissociation energies (BDE) were deduced from the thermochemical data which have been used in the model and estimated by ab initio calculations performed at the CBS-QB3 level [38] implemented in the Gaussian 09 program suite [39]. Figure 10 shows that the BDE of C-H bonds of the methyl groups in MF and DMF (85.3 and 84.8 kcal mol^{-1}, respectively) are much lower than those of the ring-carbon-CH_3 bonds (~112.9-113.4 kcal mol^{-1}) in MF and DMF, and those of the ring-carbon-H bonds (~119.3-119.6 kcal mol^{-1}) in the three fuel molecules. Therefore, the contribution of H-abstractions in fuel consumption is enhanced when going from furan to DMF. The BDE of the C-H bond in the methyl group of MF is 85.3 kcal mol^{-1}, which is in good agreement with that of 86.2±1.2 kcal mol^{-1}, theoretically calculated by Simmie and Curran [40] and with 86.4±2 kcal mol^{-1} estimated by Stein from very low pressure pyrolysis experiments [41]. Similarly, the C-H bond dissociation energy of 84.8 kcal mol^{-1} in the methyl group of DMF is in excellent agreement with that of 85.5±1.4 kcal mol^{-1}, calculated by Simmie and Curran [40]. A good agreement between our calculation and that of Simmie and Curran [40] can be also observed for other BDEs in the fuels.

CO is a primary product in the decomposition of all three fuels, as shown in Fig. 9 and in Figs. 12 of Part I [29] and Part II [30], but at a distance higher than 4 mm above the burner, most of CO is formed from several oxidation reactions of C_1-C_2 species in the reaction base. Therefore, a comparison of primary production of CO in the three flames must be done in the

early stage of reaction, below 4 mm above the burner. The distribution of the combustion products of each fuel is strongly related to the ability of a given molecule, i.e., furan, MF and DMF, to easily eliminate CO via its initial radicals in the flame. While furan and MF feature hydrogen atom(s) in position 2 and 5, and position 5, respectively, allowing the elimination of CO in a few elementary reactions, the presence of two methyl groups in DMF forbids any easy CO-elimination. The comparison of the mole fraction profiles of CO in Fig. 11 and in Fig. S7 (provided in the Supplemental Material) for the three different fuels is a good illustration of this structure-driven behavior, with the observed mole fraction of CO close to the burner following the order $CO_{(furan)}>CO_{(MF)}>CO_{(DMF)}$.

C_2H_2 is also a primary product in the decomposition of all three fuels. The profiles of C_2H_2 display a marked maximum at a distance above the burner where several reactions in the reaction base contribute for a large part to the formation of C_2H_2. An ROP analysis in the early stage of reaction, below 3 mm above the burner, shows the following characteristics: In the furan flame most of C_2H_2 comes from the direct consumption pathway of fuel (mostly by H-addition on C2 or C5 positions), while in the MF flame, excluding the direct consumption pathway of fuel, about 50% of C_2H_2 is formed via the formation of furan. Similarly, in the DMF flame, about 50% of C_2H_2 is obtained through the formation of MF and furan. This requirement of a pathway through formation of stable molecules lowers the formation of C_2H_2 in the DMF flames compared to MF and furan combustion. As seen in Fig. 11, the experimental and computed mole fraction of acetylene (C_2H_2), in the early stage of reaction, is the largest in the furan flame, followed by those in the MF and DMF flames. Note that a slight lower maximum value of computed C_2H_2 profile in the furan flame could result from probable uncertainties in the rate constants of some reactions (yielding C_2H_2) in the reaction base or from the effect of uncertainties in the temperature measurement.

The mole fraction profiles of C_2H_6 are directly related to the mole fractions of methyl radicals released in the system (mostly by ipso-reactions for methylated furans) and C_2H_6 formation is therefore also dependent on the fuel structure. In the case of furan, the methyl radical is mostly produced subsequently to the CO-elimination after the ring opening of the dihydrofuryl-3 radical. Thus, the mole fraction of C_2H_6 (Fig. 11) follows the sequence $C_2H_{6(DMF)}>C_2H_{6(MF)}>C_2H_{6(furan)}$.

The 1,3-butadiene (1,3-C_4H_6) formation in MF and DMF comes from a competitive decomposition route to the ipso-elimination (leading to furan+CH_3 and MF+CH_3, respectively). 1,3-C_4H_6 is mainly formed by the addition of H-atoms to MF and DMF, while the lack of the methyl group in furan favors the CO-elimination via the H-additions; the mole fractions are consistently noted (Fig. 11) to follow the sequence 1,3-$C_4H_{6(DMF)}$>1,3-$C_4H_{6(MF)}$>1,3-$C_4H_{6(furan)}$.

Figure 11 shows that the mole fraction of ketene (C_2H_2O) in the DMF flame is the largest, followed by those in the MF and furan flames. The ketene formation for the DMF fuel is also related to the presence of the methyl groups bound to the C2 and C5 positions, compared to the H-atom available in furan and MF (in position 5), see Fig. 10. Indeed, in the DMF flame, ketene is mainly formed by the reaction of the CH_3 and CH_3CO radicals ($CH_3CO+CH_3=C_2H_2O+CH_4$) which are produced directly from the DMF decomposition (see flow-rate analysis in Fig. 9), while this reaction plays a minor role for the ketene formation in the furan and MF flames.

Carbonyl compounds including formaldehyde, acetaldehyde, propenal, propanal and others were also measured in the flames of the three fuels. Formaldehyde (CH_2O) was the most abundant one. These aldehydes were detected with a lower mole fraction in the DMF flame than in the furan and MF flames (see Table S1) and Fig. 11 for propenal (acrolein, C_3H_4O).

As well known, cyclic species, e.g. 1,3-cyclopentadiene, benzene, toluene, and phenol play an important role in the polycyclic aromatic hydrocarbon (PAH) formation followed by soot

production. These species were measured with much higher mole fractions in the DMF flames compared to those in the furan [29] and MF flames [30], especially for 1,3-cyclopentadiene (by a factor of 10-30) and phenol (by a factor of 20-100), as seen in Fig.12 and in Table S1. In the fuel-rich flame, the maximum mole fractions of 1,3-cyclopentadiene, benzene, and phenol are 2.5×10^{-3}, 1.0×10^{-3}, and 9.1×10^{-4}, respectively, compared to 2.0×10^{-4}, 2.8×10^{-4}, and 3.4×10^{-5} in the MF flame [30], and to 1.0×10^{-4}, 1.3×10^{-4}, and 1.0×10^{-5} in the furan flame [29]. The structure of DMF versus that of MF and furan is a leading factor for this observed difference in mole fractions. For DMF, the loss of CO and an H-atom will ultimately lead to 1,3-C_5H_6 and the simulations for the DMF flames show that 1,3-C_5H_6 is a product of the most important reaction channels. Furan with only four carbon atoms should form 1,3-C_5H_6 from build-up reactions. Also, the MF reaction flow analysis in [30] does not show this compound as a major product obtained directly from the fuel. Again, the presence of the methyl groups in position 2 and 5 in DMF (Fig. 10) forbids any primary channels leading to an easy elimination of CO. Therefore, several subsequent rearrangements are necessary before the fuel can break into smaller fragments. In the case of DMF, CO is ultimately eliminated after the formation of R5-, R-7, and R9-C_6H_7O with the formation of C_5H_7 radicals. However, a large part of the simulated 1,3-C_5H_6 mole fraction results from the decomposition of phenol and the cyclohexadienones (M2C_6H_6O and M3C_6H_6O) which are the major primary precursor molecules.

The combination of two resonance-stabilized propargyl radicals (C_3H_3) yields benzene or an H-atom and the phenyl radical (C_6H_5). The latter then combines with an H-atom to form benzene. Benzene can also be formed from the $C_4H_4+C_2H_3$ reaction. These reaction pathways are the principal pathways of benzene formation in furan [29] and MF [30] flames, while in the DMF flames, the reaction of phenol with an H-atom ($C_6H_6O+H=C_6H_6+OH$) contributes additionally for a large part (>60%) to the formation of benzene. Therefore, benzene is detected

with the largest mole fraction in the DMF flames in comparison to furan and MF flames, as shown in Fig. 12.

Toluene (not shown in Fig.12) is mainly formed from the combination of the methyl (CH_3) and phenyl (C_6H_5) radicals which can be formed from the combination of two C_3H_3 radicals but also from H-abstractions from benzene. As discussed above, benzene is formed with a larger mole fraction in the DMF flames, therefore toluene exhibits a similar trend.

The above comparison shows that the combustion of DMF has a higher ability to form soot precursors (e.g. 1,3-cyclopentadiene or benzene), compared to that of furan and MF. Note that Djokic et al. [42] also recently pointed out the high tendency of DMF to form large amounts of soot precursors from their experimental study of the thermal decomposition of DMF.

6.2. Comparison of the three fuels with selected others

It is also thought to be very interesting to compare fuel-rich flames of these furanic fuels with those of some selected fuels in the literature regarding the formation of potential pollutants. In addition to the flames studied in this series, flames of n-butane [32], 1-butene [43], cyclohexane [44], dimethylether [45], ethanol [8], 1-butanol [31], and methyl propanoate [46] are considered for this discussion. All these studies have been performed under premixed low-pressure flame conditions using the same analytical technique (MBMS) as the present study. Flame conditions are not exactly the same for all these studies, but approximately comparable. Therefore, it is possible to compare the order of magnitude of the amount of some compounds. Note that for the ethanol flame, the comparison is performed at an equivalence ratio of 2.57, which is much higher than that for other flames; therefore, the stoichiometric flame condition is also presented for this fuel.

Special emphasis is placed on soot precursors including acetylene, propargyl radical, 1,3-butadiene, 1,3-cyclopentadiene, and benzene, and on oxygenates including formaldehyde, methanol, acetaldehyde, acrolein and phenol, which may limit the use of biofuels in terms of air

quality improvement. Therefore, it is important to provide information on these compounds which are undesired and harmful products. This comparison is illustrated in Table 5, where maximum mole fractions of three selected species are reported which were formed under approximately comparable flame conditions. The bold values highlight the highest concentration that was obtained for each pollutant. Based on these experimental data, some interesting trends were observed.

The mole fraction of acetylene produced in the furanic fuel flames is quite comparable to that detected in the flames of the C_4-C_5-hydrocarbon fuels n-butane, 1-butene, and cyclohexane, as well as to that in the 1-butanol flame (~3-4×10^{-2}), while the mole fraction of ethene measured in the furanic fuel flames (~7-8×10^{-3}) is lower than that measured in C_4-C_5 fuel flames (~2-3×10^{-2}), but similar to that detected in the flames of the C_2-oxygenated fuels dimethylether and ethanol. The propargyl radical was detected with a much larger mole fraction in the 1-butene and cyclohexane flames of ~1.0-1.6×10^{-3}, compared to those for the flames of furanic fuels, n-butane, ethanol, 1-butanol, and methyl propanoate of ~1-6×10^{-4}. The largest mole fractions of 1,3-butadiene were observed with about (0.9-1.3)×10^{-2} in the 1-butene and cyclohexane flames, followed by those in the MF and DMF flames of ~2.0-2.7×10^{-3}, which is much higher than those for other fuels where it is less than 8×10^{-4}. As presented in Section 6.1 of the present paper and in Refs. [43,44], 1,3-butadiene is an important primary product of the combustion of 1-butene, cyclohexane, MF, and DMF.

The highest mole fractions of 1,3-cyclopentadiene and benzene were detected in the DMF flame (~2.5×10^{-3} and 1.0×10^{-3}, respectively), while mole fractions of these species detected in the furan and MF flames were quite comparable to those in the 1-butene and n-butane flames. The lowest mole fractions of these soot precursors were observed in the ethanol and 1-butanol flames.

For potentially harmful oxygenated species, the highest formaldehyde mole fraction of 2.1×10^{-2} was detected in the dimethylether flame. As presented in [45], formaldehyde is an important primary product of the fuel consumption pathways in the dimethylether flame. Indeed, by H-abstraction, dimethylether is mainly consumed to form the methoxymethyl radical (CH_3OCH_2) which then decomposes by β-scission as the principal source of formaldehyde and the methyl radical. The highest acetaldehyde values of 1.7×10^{-2} were measured in the 1-butanol flame, followed by that in the ethanol flame. As discussed in [31], in the combustion of 1-butanol, acetaldehyde might originate from ethenol (C_2H_3OH) which can be produced through an important pathway of consumption of the fuel, namely H-abstraction at the α-site of the 1-butanol molecule followed by β-scission of the C-C bond. In the case of the ethanol flame, acetaldehyde is reported to be a primary product of ethanol combustion. By H-abstraction from the α-site of the ethanol molecule, the CH_3CHOH radical is produced and then quickly yields acetaldehyde by β-scission of the O-H bond or by oxidation [5,47]. The highest methanol concentrations of 2.3×10^{-3} were found in the methyl propanoate flame, the highest acrolein values of 2.5×10^{-3} in the furan flame, and the highest phenol values of 6.3×10^{-4} in the DMF flame. The discussion about the formation of acrolein and phenol in the furanic fuel flames has been presented in Section 6.1.

On the whole, regarding the formation of pollutants for the different fuels reported in Table 5, it is clear that there is no fuel which can be considered fully "clean" under these conditions. As expected, it is seen that most acyclic oxygenated fuels tend generally to produce lower amounts of soot precursors than hydrocarbon fuels; with oxygenated-unsaturated-cyclic compounds such as furanic fuels, the potential of soot precursor formation is mostly close to that of hydrocarbon fuels. Moreover, the formation of 1,3-cyclopentadiene, benzene and phenol in the DMF flame is much higher. This unexpected trend is also predicted by the model in this series

([29,30] and the present work), and should be kept in mind before a further usage of furanics, especially DMF, as transportation fuels.

7. Summary and conclusion

In this work, experimental results for two premixed laminar flames of 2,5-dimethylfuran were presented as part of a series of three papers; the experiments were accompanied with simulations using a single detailed kinetic mechanism which allowed to reproduce the combustion of furan and the alkylated furans 2-methylfuran, and 2,5-dimethylfuran. The identification and quantitative concentration measurement of about 60 species as a function of burner distance, including stable, radical, and isomeric species, has been made possible by a powerful combination of EI-MBMS and GC which provides insight into the specific combustion mechanisms for the three fuels. The overall agreement between experiments and simulations is quite satisfactory for major species and especially also for the primary fuel consumption products.

While it is the first time that a single kinetic model has been used to simulate the combustion of these three potential alternative fuels, details in the combustion mechanism and in the measurements, including more precise rate coefficients as well as ionization energies for some of the important intermediates along the main combustion pathways leave ample room for improvement.

Considering first the comparison of the present results and those obtained for the combustion of furan and 2-methylfuran, as well as for some other selected fuels previously studied under approximately conditions, the following observations can be drawn regarding the formation of potential pollutants:

- Among all intermediate species measured for the three furanic fuels, the production of acetylene is the largest, especially in the flame of furan.

- The a priori surprising ability of DMF to form soot precursors (e.g. 1,3-cyclopentadiene and benzene) compared to the less substituted furans and to other types of fuels (e.g. alkanes and alkenes) has been experimentally observed and is well explained in the model.
- Carbonyl species including formaldehyde, acetaldehyde, acrolein (propenal), and propanal were detected with a lower mole fraction in the DMF flames than in the furan and MF flames. Furanic fuels lead to lower amounts of saturated aldehydes than 1-butanol, but to much more acrolein.

Acknowledgments

CT and DL thank the Alexander von Humboldt foundation for their research fellowships. The authors thank Patrick Nau, Julia Koppmann, and Alexander Lackner for their assistance with the temperature measurements and Regine Schröder for her assistance in preparing the manuscript. LST and DF were in part supported under the STSM program of COST Action CM 0901. The LRGP group was supported by the European Commission ("Clean ICE" ERC Advanced Research Grant) and was also granted access to the HPC resources of CINES under the allocation C2013086686 made by GENCI (Grand Equipement National de Calcul Intensif).

References

[1] A. Demirbas, Prog. Energy Combust. Sci. 33 (2007) 1–18.

[2] A.K. Agarwal, Prog. Energy Combust. Sci. 33 (2007) 233–271.

[3] T.S. Norton, F.L. Dryer, Int. J. Chem. Kinet. 24 (1992) 319–344.

[4] H.J. Curran, M.P. Dunphy, J.M. Simmie, C.K. Westbrook, W.J. Pitz, Proc. Combust. Inst. 24 (1992) 769–776.

[5] N.M. Marinov, Int. J. Chem. Kinet. 31 (1999) 183–220.

[6] M.U. Alzueta, J.M. Hernández, Energy Fuels 16 (2002) 166–171.

[7] P. Dagaut, C. Togbé, Energy Fuels 22 (2008) 3499–3505.

[8] T.S. Kasper, P. Oßwald, M. Kamphus, K. Kohse-Höinghaus, Combust. Flame 150 (2007) 220–231.

[9] N. Leplat, P. Dagaut, C. Togbé, J. Vandooren, Combust. Flame 158 (2011) 705–725.

[10] M. Mascal, E.B. Nikitin, Angew. Chem. Int. Ed. 47 (2008) 7924–7926.

[11] H. Zhao, J.E. Holladay, H. Brown, Z.C. Zhang, Science 316 (2007) 1597–1600.

[12] Y. Su, H.M. Brown, X. Huang, X.-d. Zhou, J.E. Amonette, Z.C. Zhang, Appl. Catal. A 361 (2009) 117–122.

[13] A.A. Rosatella, S.P. Simeonov, R.F.M. Frade, C.A.M. Afonso, Green Chem. 13 (2011) 754–793.

[14] Y. Román-Leshkov, C.J. Barrett, Z.Y. Liu, J.A. Dumesic, Nature 447 (2007) 982–986.

[15] R. Daniel, G. Tian, H. Xu, M.L. Wyszynski, X. Wu, Z. Huang, Fuel 90 (2011) 449–458.

[16] S. Zhong, R. Daniel, H. Xu, J. Zhang, D. Turner, M.L. Wyszynski, P. Richards, Energy Fuels 24 (2010) 2891–2899.

[17] C. Wang, H. Xu, R. Daniel, A. Ghafourian, J.M. Herreros, S. Shuai, X. Ma, Fuel 103 (2013) 200–211.

[18] M.A. Grela, V.T. Amorebieta, A.J. Colussi, J. Phys. Chem. 89 (1985) 38–41.

[19] A. Lifshitz, C. Tamburu, R. Shashua, J. Phys. Chem. A 102 (1998) 10655–10670.

[20] X. Wu, Z. Huang, T. Yuan, K. Zhang, L. Wei, Combust. Flame 156 (2009) 1365–1376.

[21] G. Tian, R. Daniel, H. Li, H. Xu, S. Shuai, P. Richards, Energy Fuels 24 (2010) 3898–3905.

[22] X. Wu, Z. Huang, X. Wang, C. Jin, C. Tang, L. Wei, C.K. Law, Combust. Flame 158 (2011) 539–546.

[23] J.M. Simmie, W.K. Metcalfe, J. Phys. Chem. A 115 (2011) 8877–8888.

[24] P. Friese, T. Bentz, M. Olzmann, J.M. Simmie, Proceedings of the European Combustion Meeting, Cardiff, 2011.

[25] B. Sirjean, R. Fournet, Proc. Combust. Inst. 34 (2013) 241–249.

[26] B. Sirjean, R. Fournet, Phys. Chem. Chem. Phys. 15 (2013) 596–611.

[27] B. Sirjean, R. Fournet, J. Phys. Chem. A 116 (2012) 6675–6684.

[28] B. Sirjean, R. Fournet, P.-A. Glaude, F. Battin-Leclerc, W. Wang, M.A. Oehlschlaeger, J. Phys. Chem. A 117 (2013) 1371-1392.

[29] D. Liu, C. Togbé, L.-S. Tran, D. Felsmann, P. Oßwald, P. Nau, P.-A. Glaude, B. Sirjean, R. Fournet, F. Battin-Leclerc, K. Kohse-Höinghaus, Combust. Flame (2013), submitted for publication.

[30] L.-S. Tran, C. Togbé, D. Liu, D. Felsmann, P. Oßwald, P.-A. Glaude, B. Sirjean, R. Fournet, F. Battin-Leclerc, K. Kohse-Höinghaus, Combust. Flame (2013), submitted for publication.

[31] P. Oßwald, H. Güldenberg, K. Kohse-Höinghaus, B. Yang, T. Yuan, F. Qi, Combust. Flame 158 (2011) 2–15.

[32] P. Oßwald, K. Kohse-Höinghaus, U. Struckmeier, T. Zeuch, L. Seidel, L. Leon, F. Mauss, Z. Phys. Chem. 225 (2011) 1029–1054.

[33] E. Pousse, P.A. Glaude, R. Fournet, F. Battin-Leclerc, Combust. Flame 156 (2009) 954–974.

[34] C. Morley. Gaseq V063, Program for thermodynamic gas equation, 1999.

[35] R.J. Kee, F.M. Rupley, J.A. Miller, CHEMKIN II: A Fortran Chemical Kinetics Package for the Analysis of Gas-Phase Chemical Kinetics, Report No. SAND89-8009, Sandia National Laboratories, 1989.

[36] S.J. Klippenstein, L.B. Harding, Y. Georgievskii, Proc. Combust. Inst. 31 (2007) 221–229.

[37] R. Atkinson, J. Arey, Chem. Rev. 103 (2003) 4605– 4638.

[38] J.A. Montgomery, Jr., M.J. Frisch, J.W. Ochterski, G.A. Petersson, J. Chem. Phys. 110 (1999) 2822–2827.

[39] Gaussian 09, Revision B.01, M.J. Frisch, G.W. Trucks, H.B. Schlegel, G.E. Scuseria, M.A. Robb, J.R. Cheeseman, G. Scalmani, V. Barone, B. Mennucci, G.A. Petersson, H. Nakatsuji, M. Caricato, X. Li, H.P. Hratchian, A.F. Izmaylov, J. Bloino, G. Zheng, J.L. Sonnenberg, M. Hada, M. Ehara, K. Toyota, R. Fukuda, J. Hasegawa, M. Ishida, T. Nakajima, Y. Honda, O. Kitao, H. Nakai, T. Vreven, J.A. Montgomery, Jr., J.E. Peralta, F. Ogliaro, M. Bearpark, J.J. Heyd, E. Brothers, K. N. Kudin, V.N. Staroverov, R. Kobayashi, J. Normand, K. Raghavachari, A. Rendell, J.C. Burant, S.S. Iyengar, J. Tomasi, M. Cossi, N. Rega, J.M. Millam, M. Klene, J.E. Knox, J.B. Cross, V. Bakken, C. Adamo, J. Jaramillo, R. Gomperts, R.E. Stratmann, O. Yazyev, A.J. Austin, R. Cammi, C. Pomelli, J.W. Ochterski, R.L. Martin, K. Morokuma, V.G. Zakrzewski, G.A. Voth, P. Salvador, J.J. Dannenberg, S. Dapprich, A.D. Daniels, Ö. Farkas, J.B. Foresman, J.V. Ortiz, J. Cioslowski, D.J. Fox, Gaussian, Inc., Wallingford CT, 2009.

[40] J.M. Simmie, H. J. Curran, J. Phys. Chem. A 113 (2009) 5128–5137.

[41] S.E. Stein in: B.D. Blaustein, B.C. Bockrath, S. Friedman (Eds.), New Approaches in Coal Chemistry, American Chemical Society, 1981, p. 97–129.

[42] M. Djokic, H.-H. Carstensen, K.M. Van Geem, G.B. Marin, Proc. Combust. Inst. 34 (2013) 251–258.

[43] M. Schenk, L. Leon, K. Moshammer, P. Oßwald, T. Zeuch, L. Seidel, F. Mauss, K. Kohse-Höinghaus, Combust. Flame 160 (2013), 487–503.

[44] W. Li, M.E. Law, P.R. Westmoreland, T. Kasper, N. Hansen, K. Kohse-Höinghaus, Combust. Flame 158 (2011) 2077–2089.

[45] J. Wang, M. Chaos, B. Yang, T.A. Cool, F.L. Dryer, T. Kasper, N. Hansen, P. Oßwald, K. Kohse-Höinghaus, P.R. Westmoreland, Phys. Chem. Chem. Phys. 11 (2009) 1328–1339.

[46] B. Yang, C. K. Westbrook, T. A. Cool, N. Hansen, K. Kohse-Höinghaus, Z. Phys. Chem. 225 (2011) 1293–1314.

[47] L.-S. Tran, P.-A. Glaude, R. Fournet, F. Battin-Leclerc, Energy Fuels 27 (2013) 2226-2245.

[48] K.N. Joshipura, M. Vinodkumar, U.M. Patel, J. Phys. B: At. Mol. Opt. Phys. 34 (2001) 509–519.

[49] O.J. Orient, S.K. Srivastava, J. Phys. B: At. Mol. Opt. Phys. 20 (1987) 3923–3936.

[50] W.L. Fitch, A.D. Sauter, Anal. Chem. 55 (1983) 832–835.

[51] Y.-K. Kim, K.K. Irikura, M.E. Rudd, M.A. Ali, P.M. Stone, J.S. Coursey, R.A. Dragoset, A.R. Kishore, K.J. Olsen, A.M. Sansonetti, G.G. Wiersma, D.S. Zucker, M.A. Zucker, Electron-Impact Cross Sections for Ionization and Excitation, http://physics.nist.gov/PhysRefData/Ionization/Xsection.html

[52] H. Nishimura, H. Tawara, J. Phys. B: At. Mol. Opt. Phys. 27 (1994) 2063–2074.

Table 1

Flow conditions for dimethylfuran (DMF) flames; SLM: Standard liter per minute.

	ϕ	Burner diameter (mm)	Gas flow (SLM)			Pressure (mbar)	C/O ratio	Dilution	Flow velocity at T=333 K[#] (cm s^{-1})
			DMF	O_2	Ar				
Bielefeld	1.0	64	0.27	2.01	2.28	20	0.38	50%	146
	1.7	64	0.42	1.86	2.28	40	0.61	50%	73
Nancy	1.7	60	0.37	1.63	2.00	40	0.61	50%	73

[#] The flow velocity is referred to the temperature of the burner surface (cooling water).

Table 2

Intermediate species identification with EI-MBMS in dimethylfuran experiments. *M*: nominal mass, *E*: electron energy, *IP*: ionization threshold, *h*: position of maximum, x_{max}: peak mole fraction, ϕ: equivalence ratio. Calibration methods: RICS (of reference species in parenthesis), convolution (of energy distribution and ionization cross section) or direct (cold gas calibration).

Species	*M*	*E* (eV)	*IP* (eV)	Calibrated as	Calibration method	Ref.	ϕ = 1.0		ϕ = 1.7	
							h(mm)	x_{max}	*h*(mm)	x_{max}
CH_3	15	10.5	9.84	Methyl	RICS (CH_4)	[48]	3.5	2.07E-03	3.5	1.96E-03
CH_4	16	12.0	12.61	Methane	Direct	[49]	4.0	3.44E-03	4.0	4.39E-03
C_2H_2	26	12.0	11.40	Acetylene	Direct	[50]	4.0	1.43E-02	4.0	3.08E-02
C_2H_3	27	10.5	8.25	Vinyl	RICS (C_2H_4)	[51]	3.5	5.30E-06	3.5	5.65E-06
C_2H_4	28	11.25	10.51	Ethene	Direct	[52]	3.7	5.57E-03	3.5	7.05E-03
C_2H_5	29	10.5	8.12	Ethyl	RICS (C_4H_6)	[51]	3.2	3.37E-05	3.0	2.45E-05
HCO	29	10.5	8.12	Formyl	Convolution	[51]	3.7	3.47E-05	3.5	2.52E-05
C_2H_6	30	12.0	11.52	Ethane	Direct	[52]	3.2	2.79E-03	2.5	3.00E-03
CH_2O	30	11.25	10.88	Formaldehyde	Convolution	[52]	3.7	3.92E-03	3.0	2.91E-03
CH_4O	32	11.25	10.23	Methanol	Direct	[52]	1.0	3.50E-04	1.5	3.06E-04
C_3H_3	39	10.5	8.67	Propargyl	RICS (C_3H_6)	[51]	3.7	1.60E-04	3.5	3.55E-04
C_3H_4	40	11.25	10.36	Propyne	RICS (C_3H_6)	[51]	3.7	2.50E-03	3.5	3.79E-03
C_3H_5	41	10.5	8.13	Allyl	RICS (C_3H_6)	[51]	3.5	1.98E-04	3.0	1.65E-04
C_2H_2O	42	10.5	9.62	Ketene	Convolution	RICS (C_2H_6O)	3.7	2.47E-03	3.0	7.52E-04
C_3H_6	42	10.5	9.73	Propene	Direct	[52]	3.2	1.29E-03	3.0	9.15E-04
C_2H_4O	44	11.25	10.23	Acetaldehyde	Direct	[50]	3.7	6.18E-04	3.5	6.74E-04
C_2H_6O	46	10.5	10.02	Dimethylether	Direct	[50]	2.5	4.96E-05	2.0	4.20E-05
C_4H_2	50	11.25	10.17	1,3-Butadiyne	Convolution	[51]	4.0	7.82E-04	4.0	4.20E-03
C_4H_4	52	10.5	9.58	1-Butene-3-yne	Convolution	[51]	4.0	1.96E-03	3.5	3.59E-03
C_4H_5	53	10.5	7.97	But-2-yn-1-yl	Convolution	RICS (C_4H_6)	0.5	4.22E-05	0.5	1.22E-04
C_4H_6	54	10.5	9.07	1,3-Butadiene	Convolution	[51]	3.5	2.39E-03	3.0	2.72E-03
C_4H_7	55	10.5	7.40	But-3-en-1-yl	RICS (1-C_4H_8)	[51]	3.0	8.10E-05	3.0	4.27E-05

Species	*M*	*E* (eV)	*IP* (eV)	Calibrated as	Calibration method	Ref.	ϕ = 1.0		ϕ = 1.7	
							***h*(mm)**	x_{max}	***h*(mm)**	x_{max}
C_4H_8	56	10.5	9.55	1-Butene	Direct	[52]	3.0	6.72E-04	3.0	4.09E-04
C_3H_4O	56	11.25	10.11	Acrolein	RICS (C_3H_6O)	[50]	3.5	1.33E-03	3.0	8.47E-04
C_3H_6O	58	10.5	9.96	Propanal	Direct	[50]	3.0	4.28E-04	2.5	1.38E-04
C_5H_4	64	10.5	9.50	1,3-Pentadiyne	RICS (C_5H_8)	[50]	4.0	3.99E-05	3.5	1.26E-04
C_5H_6	66	10,5	8.57	1,3-Cyclopentadiene	RICS (C_5H_8)	[50]	3.7	1.55E-03	3.0	2.50E-03
C_5H_7	67	10.5	7.54	3-Cyclopentenyl	Convolution	RICS (C_5H_8)	2.2	7.24E-06	3.0	1.70E-05
C_4H_4O	68	10.5	8.88	Furan	Direct	[51]	3.5	4.68E-04	3.0	4.69E-04
C_5H_8	68	10.5	8.59	1,3-Pentadiene	Convolution	[51]	3.2	2.34E-04	3.0	2.30E-04
C_4H_6O	70	10.5	9.65	2-Butenone	Convolution	RICS (butanal)	3.2	4.42E-04	2.9	2.43E-04
C_5H_{10}	70	10.5	9.04	2-Pentene	RICS (C_5H_8)	[50]	3.0	1.01E-04	2.5	6.92E-05
C_4H_8O	72	10.5	9.52	2-Butanone	Convolution	RICS (butanal)	3.2	3.21E-05	2.5	1.24E-05
C_6H_2	74	10.5	9.50	Triacetylene	Convolution	[51]	4.0	9.02E-06	4.0	1.30E-04
C_6H_4	76	10.5	9.03	Benzyne	Convolution	RICS (C_6H_2)	4.0	1.15E-05	4.0	5.46E-05
C_6H_6	78	10.5	9.24	Benzene	Direct	[51]	4.0	3.60E-04	3.5	1.00E-03
C_6H_8	80	10.5	8.82	1,4-Cyclohexadiene	Convolution	RICS (C_6H_6)	3.2	1.42E-04	3.0	3.08E-04
C_5H_6O	82	10.5	8.37	2-Methylfuran	Convolution	RICS (furan)	3.2	2.29E-03	3.0	2.35E-03
C_5H_8O	84	10.5	9.39	3-Pentene-2-one	Convolution	RICS (acetone)	3.0	7.95E-05	3.0	4.09E-05
C_7H_8	92	10.5	8.82	Toluene	Convolution	RICS (C_6H_6)	3.7	4.31E-05	4.0	4.59E-05
C_6H_6O	94	10.5	8.49	Phenol	Convolution	RICS (C_6H_6)	3.5	6.43E-04	3.0	9.05E-04

Table 3

Comparison of maximum mole fractions (GC/MBMS/Model) for some intermediates in the DMF/O_2/Ar flame, ϕ=1.7.

Formula	Species	x_{max} (GC)	x_{max} (Model)	x_{max} (MBMS)
C_2H_2	Acetylene	2.95E-02	3.02E-02	3.08E-02
C_2H_6	Ethane	4.61E-03	4.76E-03	3.00E-03
C_3H_4	Propyne	1.48E-03	1.01E-03	3.79E-03
	Allene	0.75E-03	0.54E-03	
C_3H_6	Propene	1.11E-03	5.75E-04	9.20E-04
C_4H_4	1-Butene-3-yne	4.30E-03	1.11E-03	3.59E-03
C_4H_6	1,3-Butadiene	3.03E-03	3.35E-03	2.72E-03
	1,2-Butadiene	2.07E-04	1.36E-04	
	2-Butyne	8.82E-05	8.16E-05	
C_4H_8	1-Butene	5.00E-04	1.22E-04	4.09E-04
	2-Butene	9.09E-05	14.7E-05	
C_5H_6	1,3-Cyclopentadiene	5.02E-03	2.34E-03	2.50E-03
	1-Pentene-3-yne	1.18E-04	a	
C_5H_8	1,3-Pentadiene trans	3.33E-04	0.60E-04	2.30E-04
	Isoprene	3.03E-05	0.24E-04	
	2-Pentyne	3.67E-05	1.04E-04	
C_5H_{10}	2-Pentene	2.89E-04	2.37E-04	6.92E-05
	3-Methyl-1-butene	5.68E-05		
	1-Pentene	b	1.70E-05	
C_6H_6	Benzene	1.25E-03	0.23E-03	1.00E-03
C_7H_8	Toluene	12.10E-05	9.11E-05	4.59E-05[e]
C_2H_4O	Acetaldehyde	4.24E-04	14.60E-04	6.74E-04
	Ethylene oxide	Trace	1.07E-04	
C_2H_6O	Dimethylether	5.77E-05	8.58E-05	4.20E-05
	Ethanol	c	a	
C_3H_6O	Propanal	5.60E-05	19.9E-05	13.80E-05
	Acetone (impurity~5E-05)	6.55E-05	10.1E-05	
C_4H_4O	Furan	d	12.30E-04	4.69E-04
C_4H_6O	2-Butenone	9.73E-04	a	2.43E-04
	2-Butenal	5.53E-05	a	
	2,3-Dihydrofuran	2.10E-05	1.08E-05	
	Iso-butenal	c	a	
C_4H_8O	2-Butanone	2.24E-05	a	1.24E-05
	Isobutanal	c	a	
C_5H_6O	2-Methylfuran (MF)	3.33E-03	4.00E-03	2.35E-03
	3-Methylfuran	2.82E-05	a	
C_5H_8O	3-Pentene-2-one	4.54E-05	a	4.09E-05

a: not available ; b: hidden by C_5H_6 peak; c: not detected; d: identified by GC/MS, but not quantified; e: taken from GC measurement

Table 4

Name and structure of some species involved in the detailed mechanism of the DMF oxidation.

Species	Name	Species	Name	Species	Name
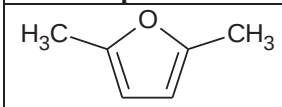	DMF	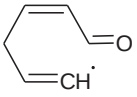	R8C_6H_7O	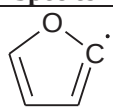	Furyl-2
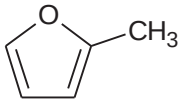	MF	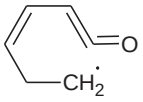	R9C_6H_7O	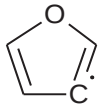	Furyl-3
	Furan	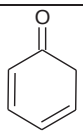	M2C_6H_6O	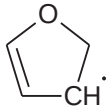	C_4H_5O-3
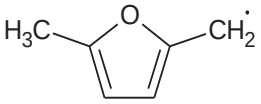	R1C_6H_7O	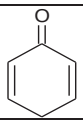	M3C_6H_6O	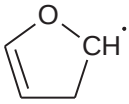	C_4H_5O-2
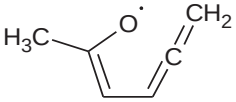	R2C_6H_7O	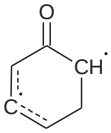	B1C_6H_6O	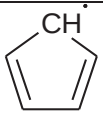	C_5H_5#
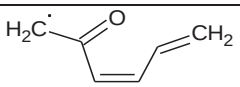	R3C_6H_7O	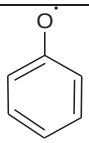	C_6H_5O#	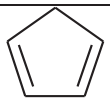	1,3-C_5H_6
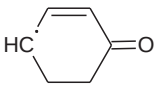	R4C_6H_7O	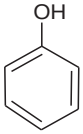	C_6H_6O	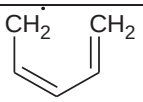	C_5H_7Y
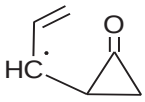	R5C_6H_7O	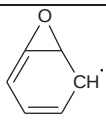	Bicycle	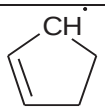	C_5H_7#Y
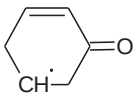	R6C_6H_7O	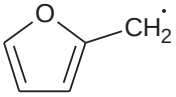	furylCH_2	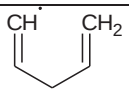	C_5H_7-1s
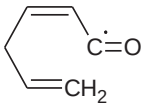	R7C_6H_7O	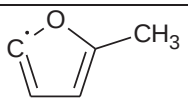	M5F-2yl	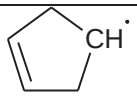	C_5H_7#

Table 5

Comparison of maximum mole fractions for potential pollutants in flames of furanic fuels with those of other fuels.

	Furan [29]	MF [30]	DMF[a]	n-Butane [32]	1-Butene [43]	Cyclohexane [44]	Dimethylether [45]	Ethanol [8]		1-Butanol [31]	Methyl propanoate [46]
Formula of fuel	 (C_4H_4O)	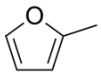 (C_5H_6O)	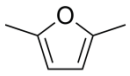 (C_6H_8O)	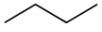 (C_4H_{10})	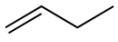 (C_4H_8)	 (C_6H_{12})	 (C_2H_6O)	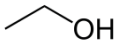 (C_2H_6O)		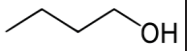 ($C_4H_{10}O$)	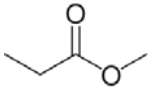 ($C_4H_8O_2$)
ϕ	1.7	1.7	1.7	1.71	1.7	2.0	1.63	1.0	2.57	1.7	1.56
Dilution	50%	50%	50%	25%	25%	30%	~26%	25%	25%	25%	25%
Pressure (mbar)	40	40	40	40	40	40	~33	50	50	40	40
Acetylene	3.5E-02	3.3E-02	3.1E-02	4.1E-02	3.9E-02	**4.2E-02**	3.9E-03	4.8E-04	8.3E-03	3.1E-02	1.6E-02
Ethene	6.7E-03	8.0E-03	7.1E-03	**3.5E-02**	2.3E-02	2.5E-02	5.0E-03	2.1E-03	8.1E-03	3.1E-02	2.6E-02
Propargyl	1.0E-04	2.5E-04	3.6E-04	2.3E-04	1.0E-03	**1.6E-03**	-	-	6.7E-04	3.4E-04	2.4E-04
1,3-Butadiene	4.6E-04	2.0E-03	2.7E-03	7.9E-04	8.5E-03	**1.3E-02**	-	-	-	7.5E-04	7.6E-05
1,3-Cyclopentadiene	1.0E-04	2.0E-04	**2.5E-03**	7.2E-05	2.6E-04	6.1E-04	-	-	-	7.5E-05	-
Benzene	1.3E-04	2.8E-04	**1.0E-03**	5.2E-05	1.6E-04	5.1E-04	-	-	7.0E-06	4.5E-05	-
Formaldehyde	3.8E-03	3.3E-03	2.9E-03	3.8E-03	4.8E-03	1.6E-02	**2.1E-02**	5.1E-03	9.4E-03	7.1E-03	1.4E-02
Acetaldehyde[b]	3.2E-03	6.1E-04	6.7E-04	3.9E-04	8.4E-04	-	5.0E-04	4.8E-03	8.8E-03	**1.7E-02**	1.8E-03[c]
Acrolein	**2.5E-03**	1.4E-03	8.5E-04	-	-	-	-	-	-	-	-
Methanol	4.4E-04	1.4E-04	3.1E-04	-	-	-	1.3E-03	-	-	-	**2.3E-03**
Phenol	9.7E-06	3.7E-05	**9.1E-04**	-	-	-	-	-	-	-	-

-: not available.

[a] present paper.

[b] probably sum of acetaldehyde and ethenol (vinyl alcohol).

[c] only acetaldehyde.

Figure captions

Figure 1. Main species mole fraction x_i and temperature T profiles as a function of height above burner h. Symbols: experiment (EI-MBMS), lines: model results. Equilibrium values (open symbols) are indicated at h=43 mm. Perturbed temperature profiles were calibrated by QCL absorption at 25.0 mm; they were used as input parameters for the numerical simulation without any changes.

Figure 2. Mole fraction profiles of selected C_1 and C_2 species for ϕ=1.7. Symbols: experiment (EI-MBMS); lines: simulation. Mole fraction profiles for ϕ=1.0 can be found in the Supplemental Material.

Figure 3. Mole fraction profiles of selected C_3 and C_4 species for ϕ=1.7. Symbols: experiment (EI-MBMS); lines: simulation. Mole fraction profiles for ϕ=1.0 can be found in the Supplemental Material.

Figure 4. Mole fraction profiles of selected C_5 and C_6 species for ϕ=1.7. Symbols: experiment (EI-MBMS); lines: simulation. Mole fraction profiles for ϕ=1.0 can be found in the Supplemental Material.

Figure 5. Mole fraction profiles of selected C_1-C_3 oxygenated species for ϕ=1.7. Symbols: experiment (EI-MBMS); lines: simulation. Mole fraction profiles for ϕ=1.0 can be found in the Supplemental Material.

Figure 6. Mole fraction profiles of selected C_4-C_6 oxygenated species for ϕ=1.7. Symbols: experiment (EI-MBMS); lines: simulation. Mole fraction profiles for ϕ=1.0 can be found in the Supplemental Material.

Figure 7. C_4H_8 isomers (1-butene and 2-butene). Left: mole fraction profiles (sum of C_4H_8) obtained in the MBMS experiment and results of the GC analysis. Right: respective model prediction and MBMS experiment results.

Figure 8. C_5H_8 isomers (isoprene, 2-pentyne, and 1,3-pentadiene). Left: mole fraction profiles (sum of C_5H_8) obtained in the MBMS experiment and results of the GC analysis. Right: respective model prediction and MBMS experiment results.

Figure 9. Reaction flow analysis for the consumption of DMF in the fuel-rich flame (ϕ=1.7) for a distance of 3.1 mm from the burner, corresponding to a simulated temperature of 1101 K and a 73% conversion of DMF. The size of the arrows is proportional to the relative rates of consumption of a given species.

Figure 10. Structure of furan, MF, and DMF. Italic numbers: calculated bond energy (in kcal mol^{-1}); number near the atom: atom label.

Figure 11. Comparison of experimental and simulated profiles of CO, C_2H_2, C_2H_6, C_4H_6, C_2H_2O and C_3H_4O for the three fuels: Furan, MF, and DMF.

Figure 12. Comparison of experimental and simulated profiles of C_5H_6, C_6H_6O and C_6H_6 for the three fuels: Furan, MF, and DMF.

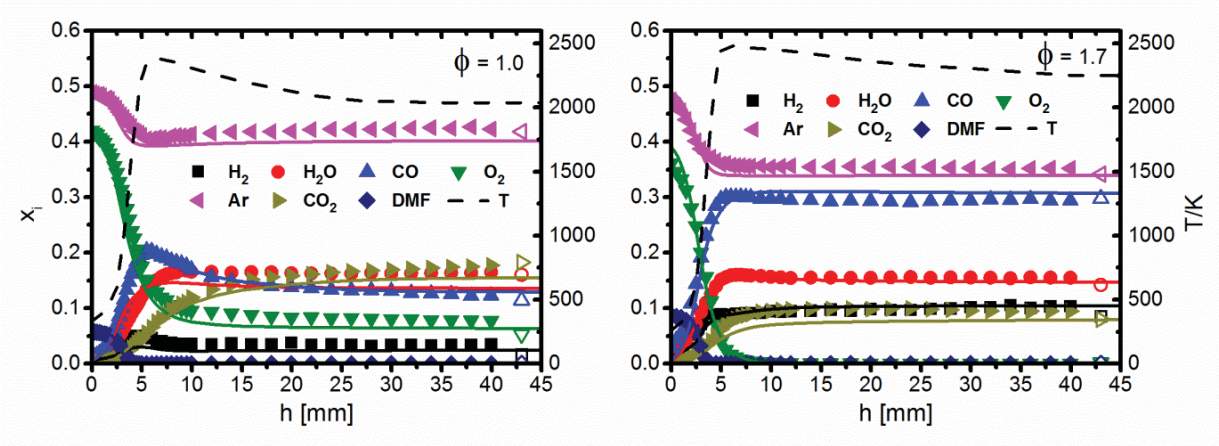

Figure 1. Main species mole fraction x_i and temperature T profiles as a function of height above burner h. Symbols: experiment (EI-MBMS), lines: model results. Equilibrium values (open symbols) are indicated at h=43 mm. Perturbed temperature profiles were calibrated by QCL absorption at 25.0 mm; they were used as input parameters for the numerical simulation without any changes.

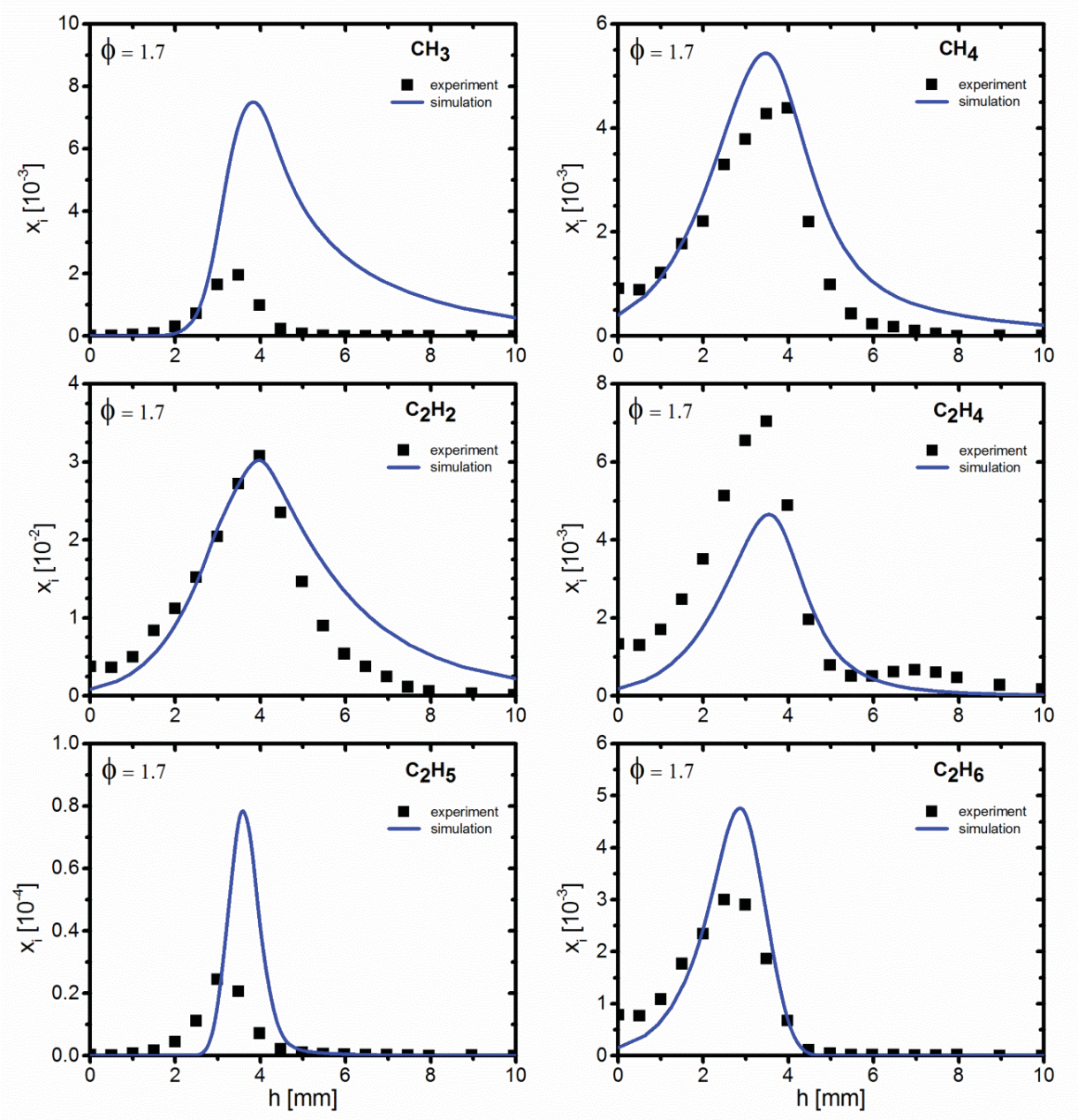

Figure 2. Mole fraction profiles of selected C_1 and C_2 species for ϕ=1.7. Symbols: experiment (EI-MBMS); lines: simulation. Mole fraction profiles for ϕ=1.0 can be found in the Supplemental Material.

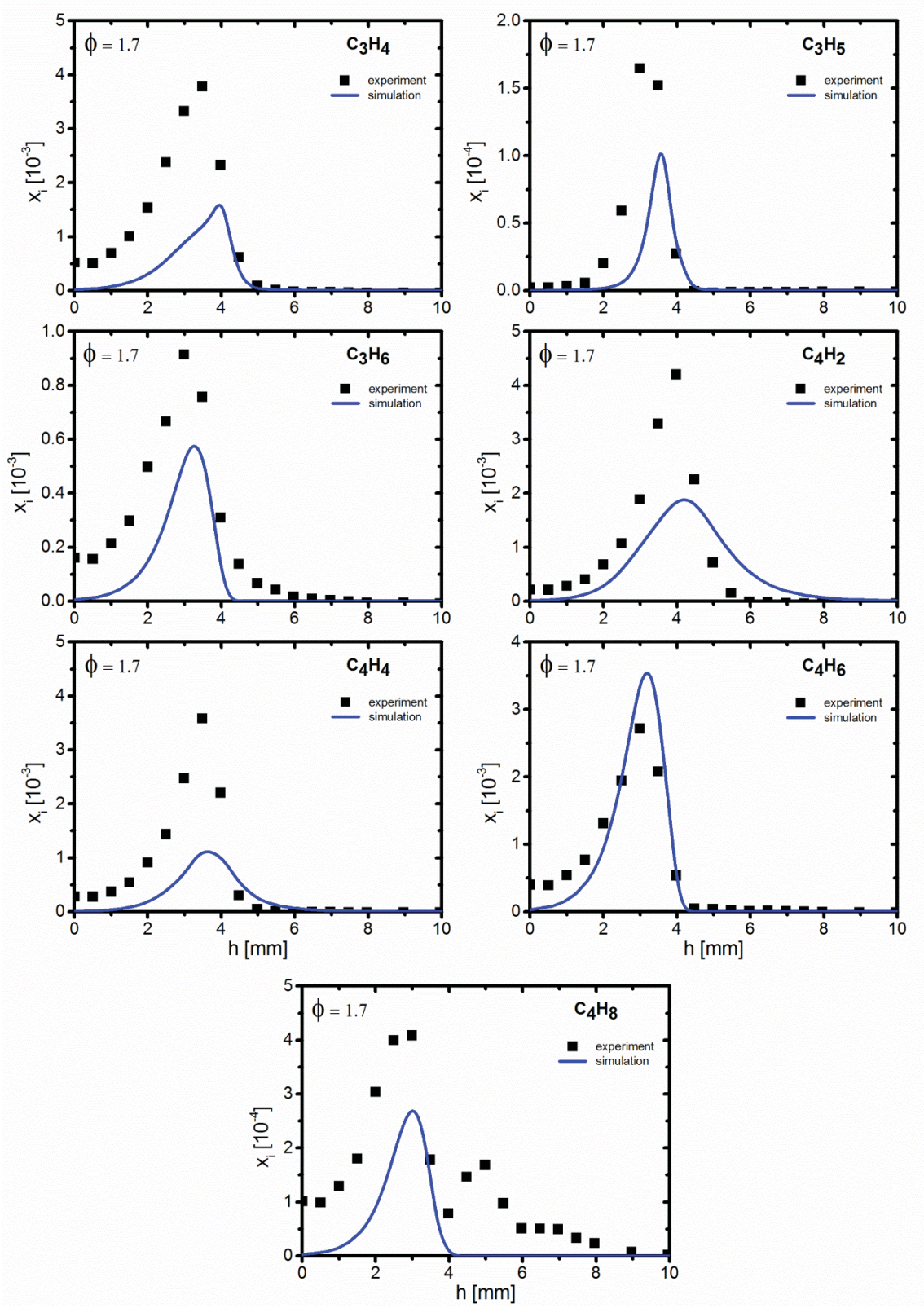

Figure 3. Mole fraction profiles of selected C_3 and C_4 species for ϕ=1.7. Symbols: experiment (EI-MBMS); lines: simulation. Mole fraction profiles for ϕ=1.0 can be found in the Supplemental Material.

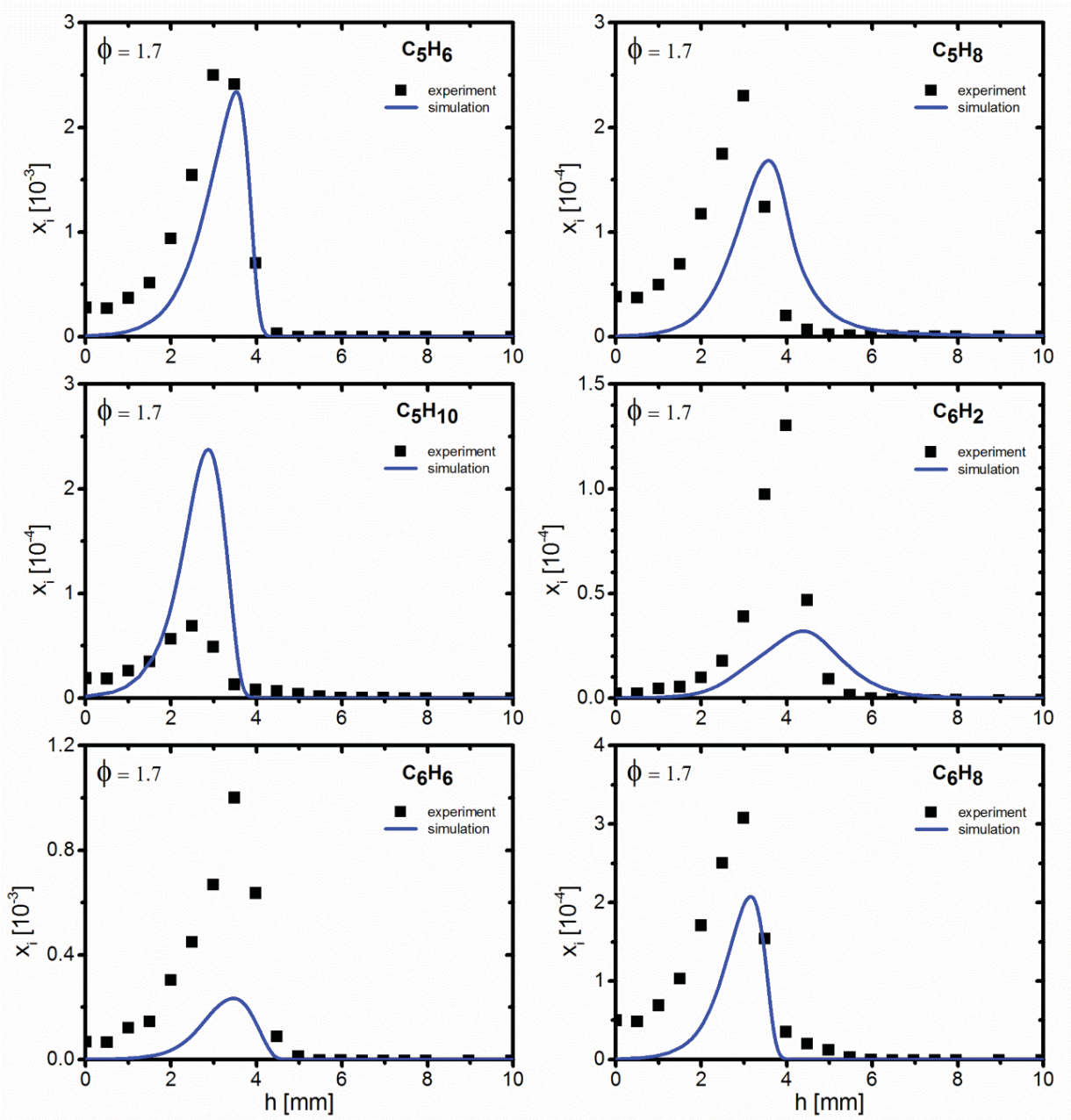

Figure 4. Mole fraction profiles of selected C_5 and C_6 species for ϕ=1.7. Symbols: experiment (EI-MBMS); lines: simulation. Mole fraction profiles for ϕ=1.0 can be found in the Supplemental Material.

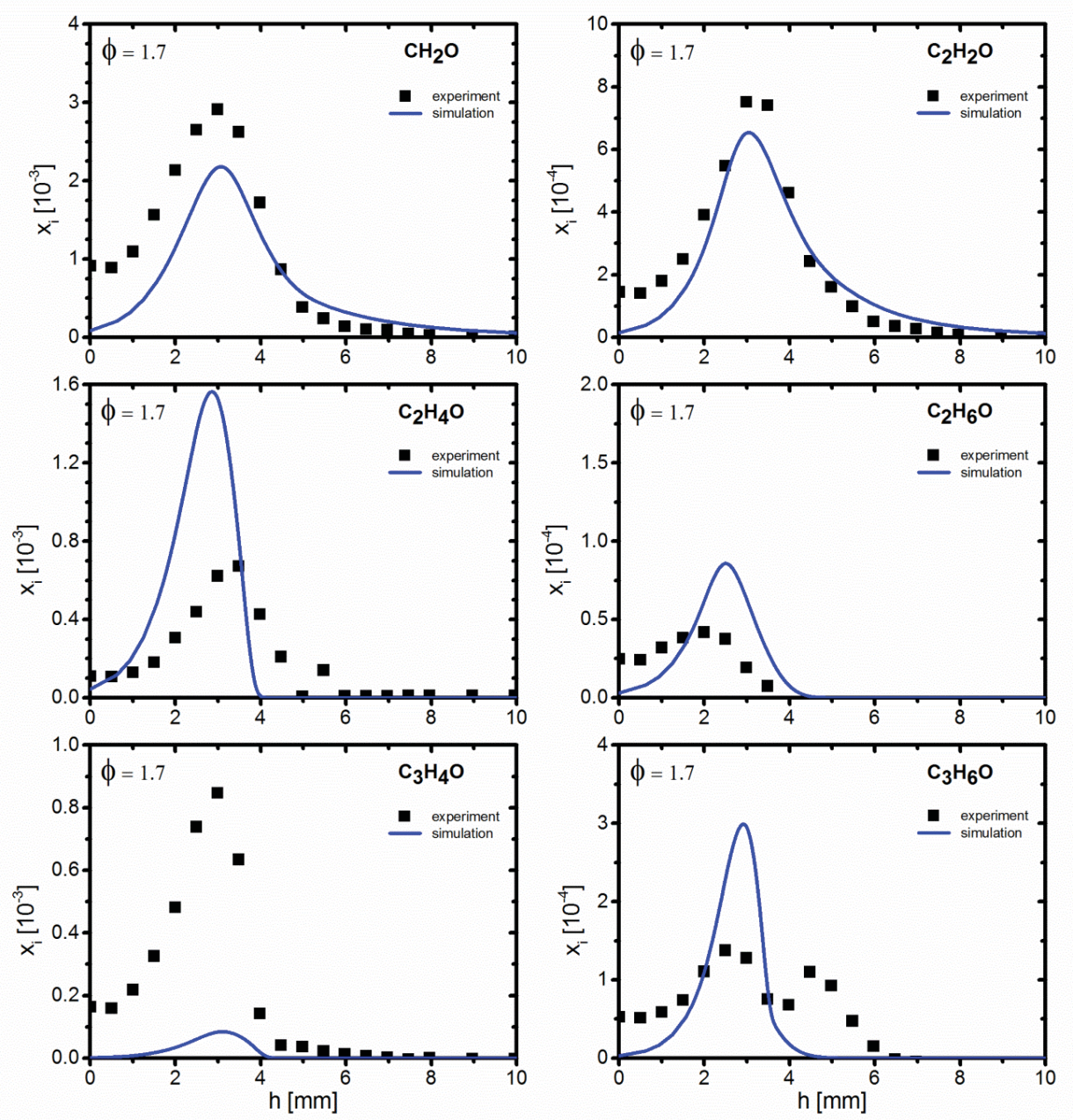

Figure 5. Mole fraction profiles of selected C_1-C_3 oxygenated species for ϕ=1.7. Symbols: experiment (EI-MBMS); lines: simulation. Mole fraction profiles for ϕ=1.0 can be found in the Supplemental Material.

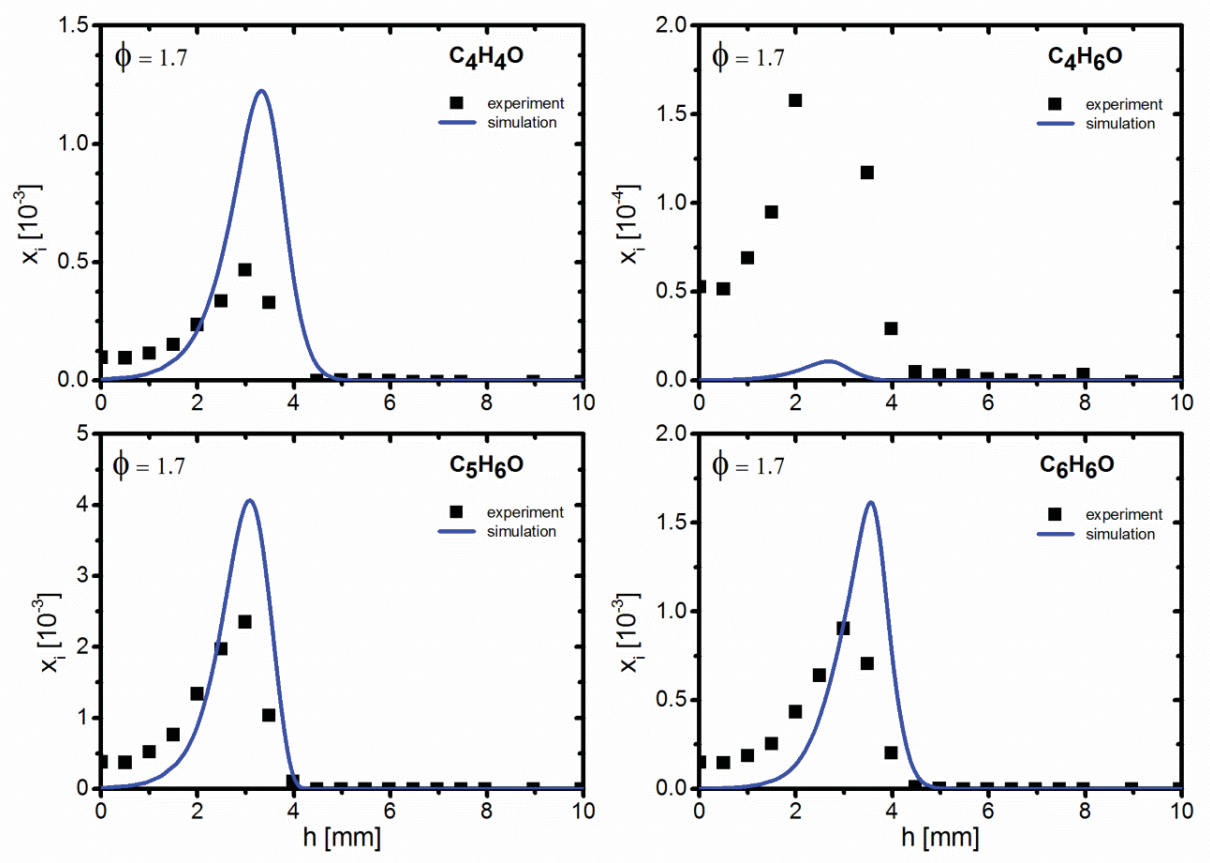

Figure 6. Mole fraction profiles of selected C_4-C_6 oxygenated species for ϕ=1.7. Symbols: experiment (EI-MBMS); lines: simulation. Mole fraction profiles for ϕ=1.0 can be found in the Supplemental Material.

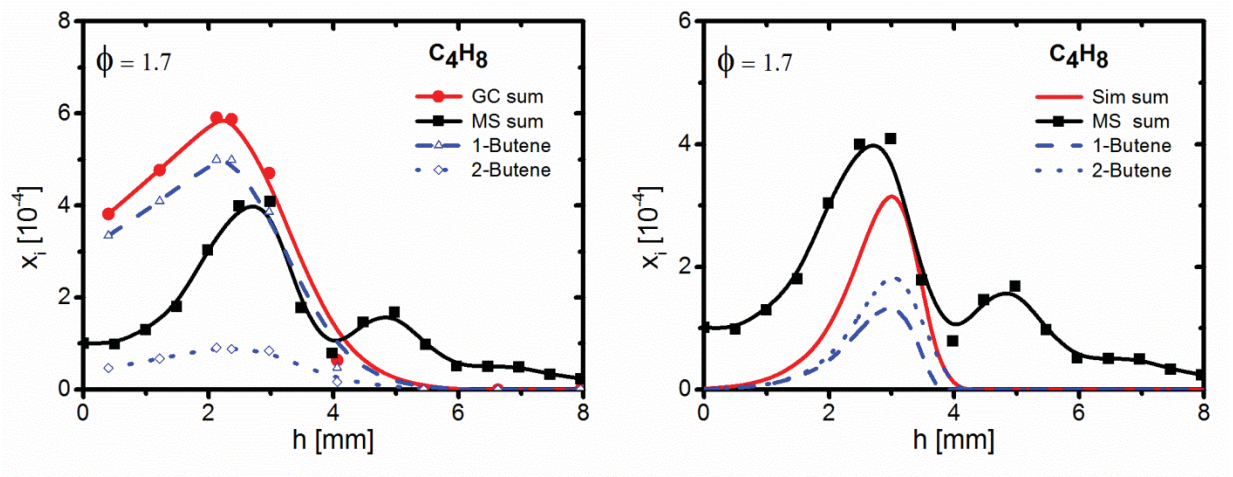

Figure 7. C_4H_8 isomers (1-butene and 2-butene). Left: mole fraction profiles (sum of C_4H_8) obtained in the MBMS experiment and results of the GC analysis. Right: respective model prediction and MBMS experiment results.

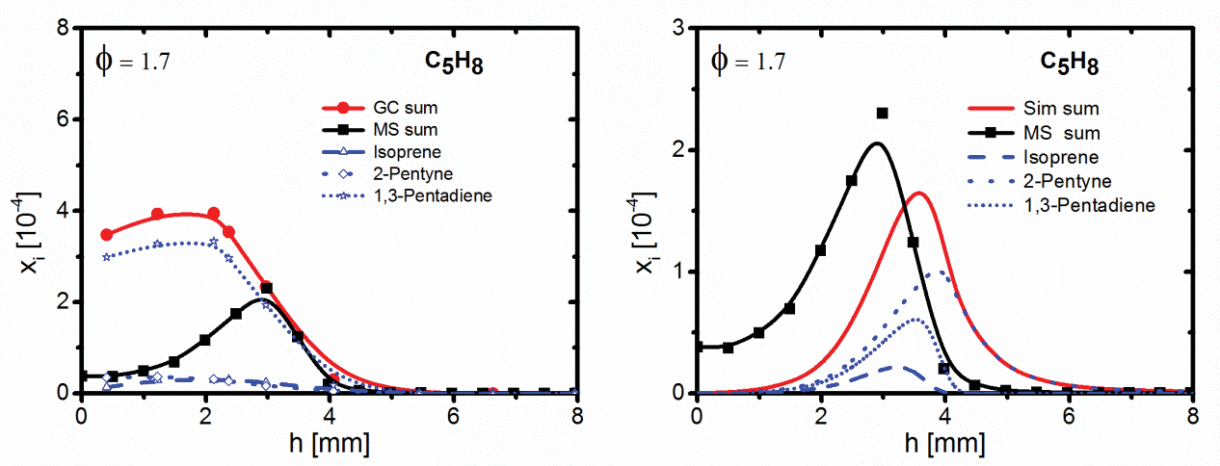

Figure 8. C_5H_8 isomers (isoprene, 2-pentyne, and 1,3-pentadiene). Left: mole fraction profiles (sum of C_5H_8) obtained in the MBMS experiment and results of the GC analysis. Right: respective model prediction and MBMS experiment results.

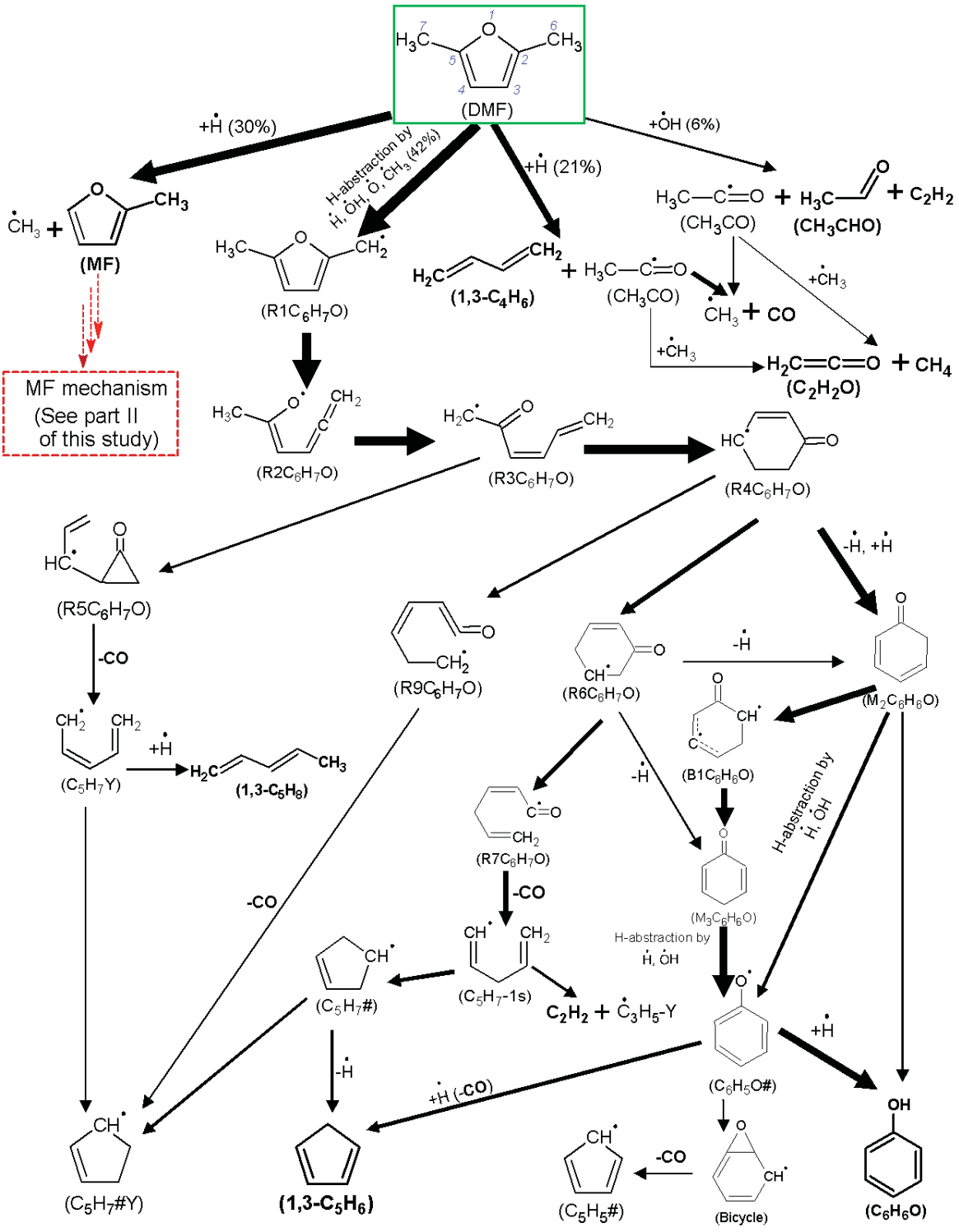

Figure 9. Reaction flow analysis for the consumption of DMF in the fuel-rich flame (ϕ=1.7) for a distance of 3.1 mm from the burner, corresponding to a simulated temperature of 1101 K and a 73% conversion of DMF. The size of the arrows is proportional to the relative rates of consumption of a given species.

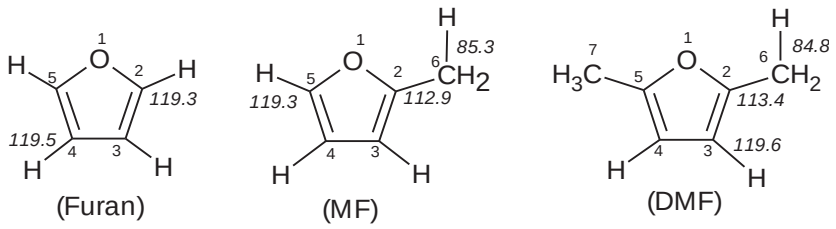

Figure 10. Structure of furan, MF, and DMF. Italic numbers: calculated bond energy (in kcal mol^{-1}); number near the atom: atom label.

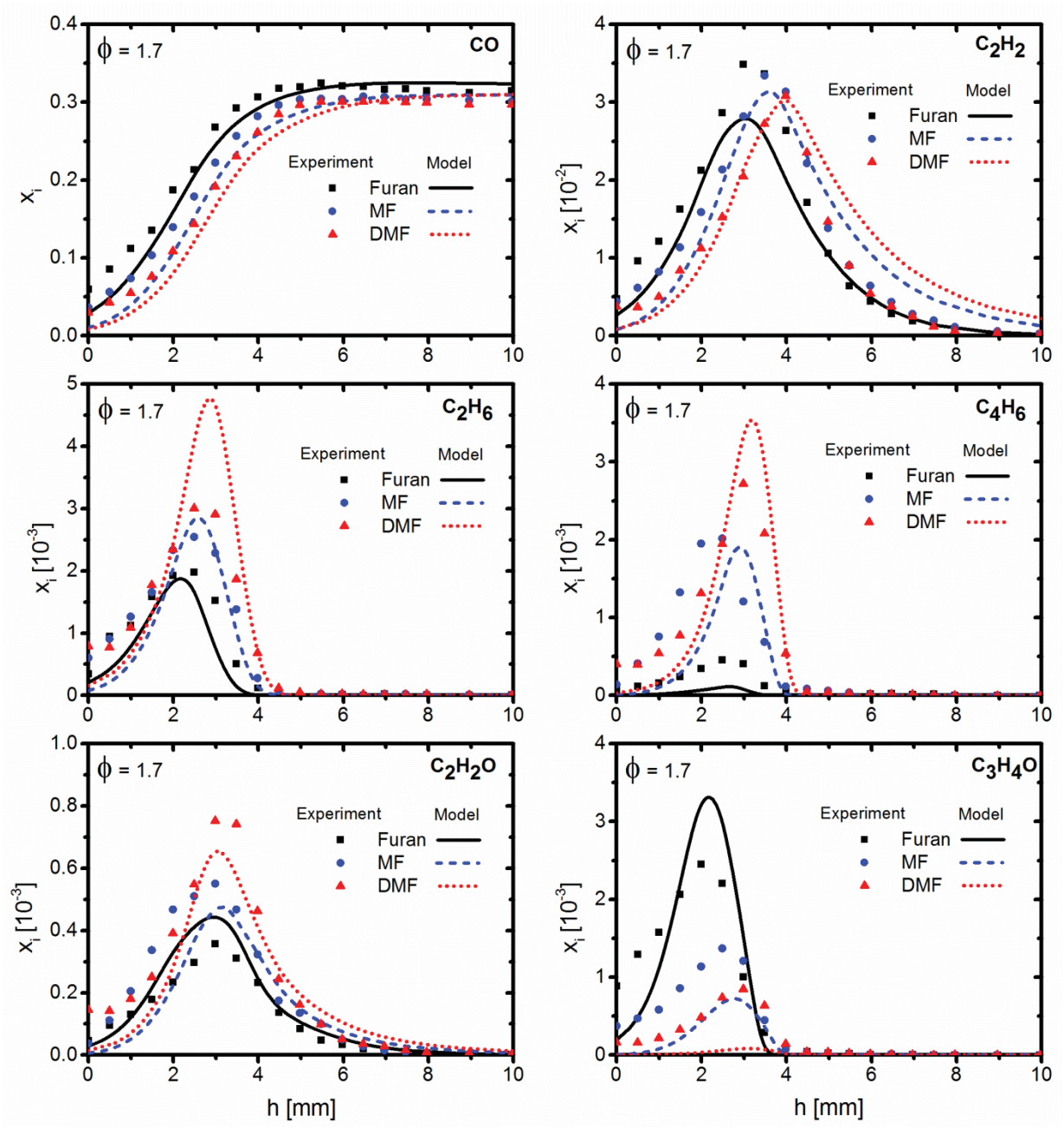

Figure 11. Comparison of experimental and simulated profiles of CO, C_2H_2, C_2H_6, C_4H_6, C_2H_2O and C_3H_4O for the three fuels: Furan, MF, and DMF.

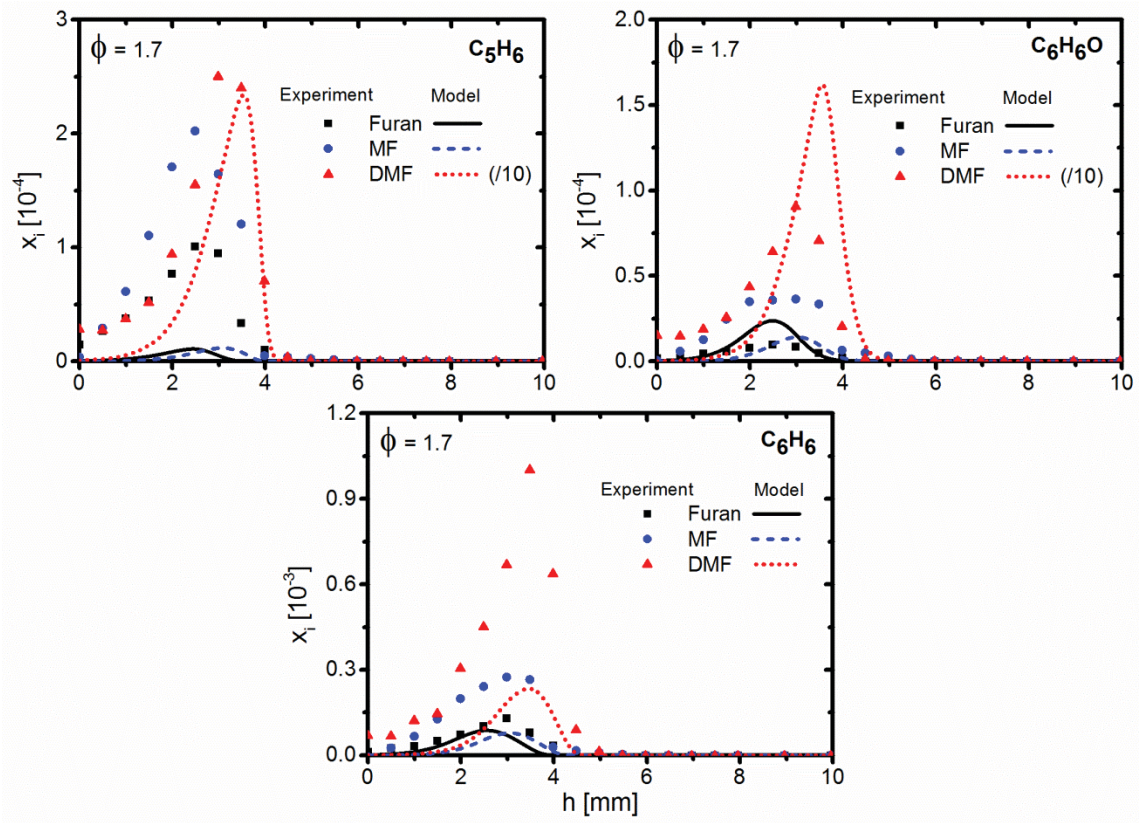

Figure 12. Comparison of experimental and simulated profiles of C_5H_6, C_6H_6O and C_6H_6 for the three fuels: Furan, MF, and DMF.